IOP Publishing Nanotechnology
Nanotechnology **28** (2017) 282002 (24pp) https://doi.org/10.1088/1361-6528/aa77ce

Topical Review

When lithography meets self-assembly: a review of recent advances in the directed assembly of complex metal nanostructures on planar and textured surfaces

Robert A Hughes[1], **Eredzhep Menumerov**[1] **and Svetlana Neretina**[1,2]

[1] College of Engineering, University of Notre Dame, Notre Dame, IN 46556, United States of America
[2] Center for Sustainable Energy at Notre Dame, Notre Dame, IN 46556, United States of America

E-mail: sneretina@nd.edu

Received 6 April 2017, revised 19 May 2017
Accepted for publication 7 June 2017
Published 22 June 2017

Abstract

One of the foremost challenges in nanofabrication is the establishment of a processing science that integrates wafer-based materials, techniques, and devices with the extraordinary physicochemical properties accessible when materials are reduced to nanoscale dimensions. Such a merger would allow for exacting controls on nanostructure positioning, promote cooperative phenomenon between adjacent nanostructures and/or substrate materials, and allow for electrical contact to individual or groups of nanostructures. With neither self-assembly nor top-down lithographic processes being able to adequately meet this challenge, advancements have often relied on a hybrid strategy that utilizes lithographically-defined features to direct the assembly of nanostructures into organized patterns. While these so-called directed assembly techniques have proven viable, much of this effort has focused on the assembly of periodic arrays of spherical or near-spherical nanostructures comprised of a single element. Work directed toward the fabrication of more complex nanostructures, while still at a nascent stage, has nevertheless demonstrated the possibility of forming arrays of nanocubes, nanorods, nanoprisms, nanoshells, nanocages, nanoframes, core–shell structures, Janus structures, and various alloys on the substrate surface. In this topical review, we describe the progress made in the directed assembly of periodic arrays of these complex metal nanostructures on planar and textured substrates. The review is divided into three broad strategies reliant on: (i) the deterministic positioning of colloidal structures, (ii) the reorganization of deposited metal films at elevated temperatures, and (iii) liquid-phase chemistry practiced directly on the substrate surface. These strategies collectively utilize a broad range of techniques including capillary assembly, microcontact printing, chemical surface modulation, templated dewetting, nanoimprint lithography, and dip-pen nanolithography and employ a wide scope of chemical processes including redox reactions, alloying, dealloying, phase separation, galvanic replacement, preferential etching, template-mediated reactions, and facet-selective capping agents. Taken together, they highlight the diverse toolset available when fabricating organized surfaces of substrate-supported nanostructures.

Keywords: capillary assembly, dewetting, dip-pen nanolithography, galvanic replacement, bimetallic nanostructures, nanomanufacturing, nanofabrication

(Some figures may appear in colour only in the online journal)

1. Introduction

Metal nanostructures are an extraordinary class of materials demonstrating unique and important physicochemical properties. An ever expanding set of synthetic pathways has given rise to an impressive collection of well-characterized nanoscale building blocks where the most notable properties are, for the most part, well-understood and often simulated. With this synthetic and mechanistic framework now in place, numerous opportunities exist for integrating these nanostructures into wafer-based devices capable of deriving new or enhanced functionalities based on the remarkable optical, chemical, thermal, magnetic, and transport properties accessible. In many instances, however, device prototyping has been stifled, not at the concept or design stage, nor for a lack of suitable nanoscale building blocks, but by the building process itself, i.e. the formation of nanostructures in the organized configurations needed to realize collective behaviors, nanostructure coupling phenomena, and interactions with adjacent bulk-scale materials.

Applications based on the collective behavior of groups of nanostructures greatly exceed those derived from individual nanostructures, and as such, there has always been the motivation to devise techniques that are able to place nanostructures into organized arrangements of one-dimensional chains [1, 2], two-dimensional assemblies [3–6], and three-dimensional clusters and supercrystals [7–13]. Two-dimensional assemblies offer one of the most intriguing possibilities as they are most readily integrated into the existing wafer-based processing science that underpins the electronics industry. From a materials science perspective, the underlying capability of this processing science is the formation of intricate patterns of dissimilar materials with well-defined properties and interfaces that collectively achieve functionality in response to external stimuli such as an applied voltage, light, heat, magnetic fields, and interactions with chemical and biological species. The potential, therefore, exists to combine existing competencies with those uniquely derived from metal nanostructures when exposed to the same stimuli. Realizing this potential, however, requires the advent of processing techniques capable of defining arbitrary patterns of nanostructures on commercially viable substrate materials in a manner responsive to the scalability, throughput, yield, and cost-effectiveness requirements synonymous with a nanomanufacturing process [14].

While the fabrication of metal nanostructures using top-down lithographic techniques provides the most obvious route toward integration with existing technologies, there exist numerous hurdles and intrinsic deficiencies that limit its effectiveness. The structures obtained through the physical vapor deposition of metal films followed by wet or dry etching processes typically yield primitive planar geometries comprised of a single element. This lack of architectural diversity rules out the use of complex three-dimensional single-crystal nanostructures known for highly tunable optical properties, facet-dependent chemical activity, and the intense plasmonic near-fields generated at sharp corners. In addition, both the polycrystalline nature of the lithographically-defined structures and the adhesion layers used to inhibit delamination from the substrate have detrimental effects on nanostructures exhibiting localized surface plasmon resonances (LSPR) [15, 16]. Moreover, readily accessible lithographic techniques have not yet demonstrated mastery over the sub-30 nm feature sizes needed to define complex nanometric objects and place them at distances promoting short-range coupling phenomena. While significant progress has been made in terms defining structures on ever smaller length-scales and even in the fabrication of three-dimensional geometries using lithographic techniques [17], such advances are accompanied by the technological and economic barriers associated with time-consuming serial processes performed on state-of-the-art instrumentation. Despite these deficiencies, top-down lithographic techniques remain unrivalled in terms of defining nanostructured arrays with true long-range order, high fidelity, and that lack a significant number of registration errors.

The spontaneous organization of colloidal nanostructures into two-dimensional assemblies provides the means for overcoming many of the deficiencies of top-down lithographic techniques. These self-assembly methods, which have been the subject of numerous reviews [3–6], allow for the use of nanostructures synthesized using the exquisite chemical and architectural controls accessible when using a colloidal chemistry that allows for seed-mediated growth modes, a nanostructure surface chemistry modulated by ligands, and a multitude of synthetic protocols able to sculpt, hollow, or deposit material onto existing structures [18–21]. The so-formed nanostructures can be quite sophisticated in terms of morphology and composition, often express a single-crystal character, and can be produced in high yield using techniques that are scalable, inexpensive, and short in duration. While the realization of two-dimensional nanostructure arrays using self-assembly techniques represent a significant triumph in nanoscale processing, inherent deficiencies often call for alternative solutions. Because these self-assembly processes are driven by short-range interactions between nanostructures [22], it precludes the possibility of assembling arrays of isolated nanostructures or groups of nanostructures (e.g., dimers, trimers) that are able to act autonomously. Even when this requirement is lifted, the assembly of defect-free arrays with true long-range order remains challenging. The assembly of asymmetric structures into ordered arrays has also proved difficult. Moreover, pattern assembly requires nanostructure mobility on the substrate surface, a property that is intrinsically connected to poor adhesion [23] and, hence, creates concerns when subjecting such structures to the post-processing steps typically required for device fabrication. The nanostructure surface ligands, which drive self-assembly processes, also prevent intimate contact between the nanostructure and substrate surface and can degrade the

performance of nanostructures in catalytic and sensing applications [24–29].

A hybrid strategy uses lithography as a means to regulate self-assembly processes. These so-called directed assembly techniques provide a promising alternative in that lithographically-defined features act as external drivers for otherwise spontaneous assembly processes. Such techniques, which lie at the crossroads where synthesis and fabrication meet, place additional controls on assembly processes that can act on length-scales extending from the nanoscale to mesoscale. The integration of these two disparate approaches brings together two mature fields and their associated capabilities to realize organized surfaces of metal nanostructures that have proven unrealizable through other means. Much of the early work in this field, which has been the subject of numerous reviews [30–41], has focused on the directed assembly of spherical or near-spherical nanostructures comprised of a single element. While these proof-of-principle demonstrations are unquestionably impressive, more recent efforts have shifted the focus toward the assembly of more sophisticated nanostructures that offer increased functionality, a focus that we expect to continue for the foreseeable future.

In this topical review, we highlight recent accomplishments in the fabrication of organized surfaces of complex metal nanostructures using directed assembly. Its scope is restricted to techniques that combine lithography and self-assembly to realize organized surfaces of complex nanostructures where the term 'complex' refers to metal nanostructures comprised of more than a single element or that deviate from a spherical (or near-spherical) geometry. We confine our discussion to techniques that are amenable to the formation of single-crystal nanostructures and to those where substrate coverage can occur over at least a $100\,\mu m^2$ in a reasonable timeframe. Directed assembly processes that utilize self-assembled structures (e.g., diblock copolymers, anodic aluminum oxide (AAO)), as opposed to lithographically-defined structures, to invoke a periodicity onto the assembly process are excluded. The techniques examined are organized into three broad categories: (i) the placement of colloidal structures at lithographically-defined target sites, (ii) the high-temperature dewetting of lithographically-defined islands or continuous films deposited on pre-patterned substrates, and (iii) liquid-phase growth modes carried out directly on the substrate using either lithographically-defined droplets containing appropriate precursors or seed-mediated growth modes carried out on periodic arrays of substrate-immobilized seeds formed using directed assembly. By focusing on an emerging area, we aim to set the stage for the many exciting breakthroughs to come.

2. Directed assembly of colloids

The transfer of nanostructures from colloidal suspensions to the substrate surface provides the most direct pathway for integrating the vast capabilities of solution-based chemistry with those of wafer-based processing. Appropriate modifications to the substrate surface can make it either resistant or receptive to nanostructure attachment [42, 43]. The lithographic patterning of such surfaces prior to their exposure to the colloid, therefore, provides the means to establish well-defined target sites capable of capturing nanostructures while leaving the remaining surface bare. The overall strategy is, hence, one where nanostructures suspended in solution populate the substrate surface in a highly deterministic manner. The role of the colloidal synthesis in this strategy is to assert the chemical controls needed to obtain monodisperse crystalline nanostructures with the desired architecture, chemical make-up, and size. The colloid must then act to supply these nanostructures to the substrate surface as discrete building blocks in sufficient quantities and on timescales commensurate with the demands of the assembly process. The role of the lithographic process is to define an engineered surface that is able to site-selectively capture colloidal structures and then through substrate-nanostructure interactions guide the structure to a predetermined orientation relative to the underlying substrate. Approaches to surface engineering include: (i) the use of wet or dry chemical etchants to create topographical features on an otherwise planar substrate, (ii) the deposition of thin films onto planar substrates followed by top-down lithographic patterning, and (iii) the fabrication of recessed regions in soft elastomeric materials using lithographically-defined stamps. Within the confines of these various approaches, there have been numerous nanostructure placement strategies devised that promote targeted placement through the use of capillary forces [44, 45], a chemically modulated surface chemistry [42, 46], electrostatic interactions [42, 47], and magnetic fields [48]. While many of these strategies have proven quite effective, we highlight in this section only those that have given rise to organized surfaces of nanostructures that meet the previously outlined review criteria.

2.1. Capillary assembly of colloids

When a drop of a colloidal suspension lands on a planar substrate, it quickly reorganizes due to surface energy considerations to form the most energetically favorable shape, a shape typically characterized by the contact angle (θ_C) formed at the three-phase vapor–liquid/suspension–substrate contact line. If the solvent component of the colloidal suspension then evaporates, it has a profound influence on the motion of the suspended particles. Differential evaporation rates across the surface of the drop give rise to a convectively driven laminar flow that, under suitable conditions, drives the suspended particles toward the contact line as the receding liquid–vapor boundary drags the collected particles in the opposing direction, a combination that leads to the pile-up of structures at the perimeter of the evaporating droplet. If, at some point, the receding contact line becomes pinned at a surface defect, then ring-shaped deposits are left behind once the remaining liquid evaporates. The phenomenon, commonly referred to as the 'coffee-ring effect' [49], is named after the ring-shaped stains formed when drops of spilled coffee evaporate.

The underlying physics governing the coffee-ring effect has been widely exploited as a mode by which to guide both

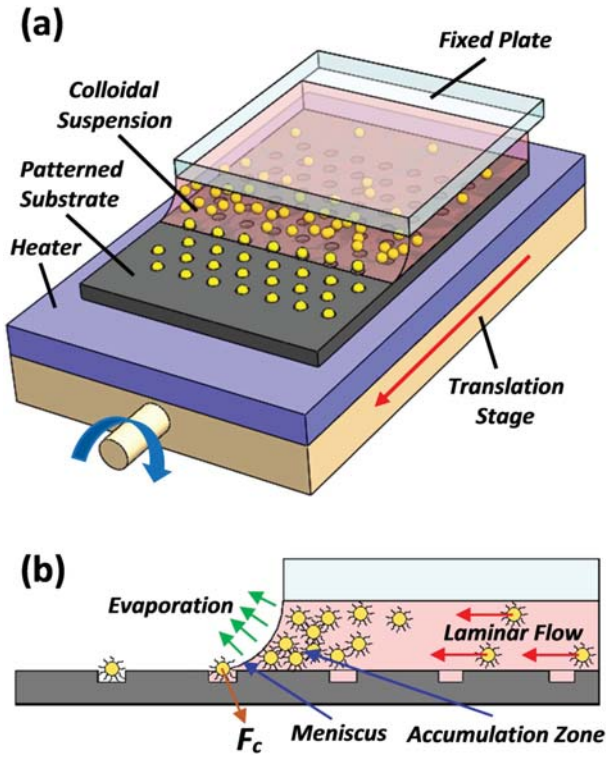

Figure 1. Schematics showing (a) the instrumentation used in the capillary assembly of colloidal nanostructures on lithographically patterned surfaces and (b) the essential mechanistic features of the assembly process that include (i) the laminar flow of nanostructures to the accumulation zone, (ii) a receding meniscus caused by evaporation and substrate translation, and (iii) nanostructures being driven into recessed features by the downward component of the capillary force ($\mathbf{F}_c$).

the self-assembly and directed assembly of suspended spherical particles [50]. Directed assembly modes utilize the receding contact line as a means to accumulate and drag large numbers of monodisperse structures over a lithographically-defined surface topography designed to pin these structures at predefined locations. Figure 1 shows schematics depicting one of the most successful strategies for obtaining organized surfaces of noble metal nanostructures [51]. This directed assembly mode relies on the confinement of a colloidal suspension between two parallel plates where the top plate is held in a fixed position as the bottom plate, i.e. a lithographically patterned substrate, is mounted on a translation stage that permits linear motion while preserving the parallel geometry. It is also important that the surface of the substrate has low-wettability, but not to the extent that it becomes hydrophobic [51, 52]. This requirement necessitates an attraction between the liquid and substrate that manifests itself as a meniscus feature whose leading edge forms a wedge-shaped geometry with the three-phase contact line (figure 1(b)) that extends across the width of the substrate. A heating element allows for the controlled evaporation of the solvent that is needed to drive the nanostructures to the contact line, and in doing so, forms a high concentration of nanostructures at the leading edge of the meniscus in what is referred to as the accumulation zone [51]. The simultaneous translation of the motorized stage at a constant velocity drags the nanostructure-containing meniscus across the substrate surface topography, allowing for suitably aligned structures to be captured in the recessed features where the capillary force exerts a downward-acting component (figure 1(b)). The directed assembly process as well as the build-up of structures in the accumulation zone can be monitored in real-time using an optical microscope under dark field illumination [53]. It is noted that a similar assembly process is also possible by simply placing drops of the colloid directly onto the same patterned substrate and allowing the solvent to evaporate [54]. While such a procedure is straightforward and quite effective in proof-of-principle demonstrations, it is less than satisfactory from the standpoint of exerting parametric control over the assembly process and in achieving assembly over large areal extents.

Like many assembly processes, the degree of success achieved when carrying out the capillary assembly of colloids is dependent on the optimization of numerous process-related parameters. Ideally, the assembly process is carried out under steady-state conditions where the number of nanostructures arriving to the accumulation zone is equaled by those trapped in the topographical features presented by the substrate. Reaching steady-state requires a conditioning period [51, 52] where the substrate is translated relative to the top plate as the accumulation zone builds. The conditions required for successful assembly relate most closely to the mechanistic aspects governing the accumulation zone and trap design.

2.1.1. Accumulation zone. The accumulation zone, in many respects, acts as a conveyor belt system for the assembly process in that it facilitates the disorganized arrival of nanoscale building blocks and sends them along a pathway in which they are packaged and compartmentalized. With nanostructure arrival being dependent on convective flows caused by solvent evaporation, it follows that the substrate temperature and the relative humidity represent key variables in the assembly process. These variables are optimized to efficiently carry nanostructures to the accumulation zone, but where the flows achieved are not so large as to cause the recirculation of nanostructures away from the zone [51]. Optimum temperatures typically reside in the range of 30 °C–50 °C. Larger values are detrimental in that they increase the level of Brownian motion experienced by the nanostructures, the results of which is a loss of structures from the accumulation zone and compromised trapping within the recesses of the substrate. The suppression of Brownian motion is, in fact, key to the assembly process [51]. A prerequisite for high-yield trapping is an accumulation zone that is densely packed with nanostructures [55]. This requirement is not merely to ensure the availability of nanostructures at the trapping site, but also restricts the mobility of the nanostructures to the extent that they are more amenable to trapping. This damping of Brownian motion becomes ever more crucial to trapping as the nanostructure size is reduced. The close confines of the nanostructures

within the accumulation zone, however, results in more demands being placed on the stabilizing ligand since nanostructure aggregation within the accumulation zone is disadvantageous to the assembly process [56]. Also key to the successful trapping of nanostructures is the shape of the meniscus [51]. If the contact angle is too high (i.e., trending toward hydrophobic), then the leading edge of the meniscus lacks the wedge-shaped geometry that is conducive to the accumulation of nanostructures. If it is to low (i.e., trending toward hydrophilic), then the assembly mode breaks down. The contact angle also plays a determining role in establishing the magnitudes of the parallel and perpendicular components of the capillary force and, hence, plays a key role in establishing the conditions needed for high-yield trapping [45]. Optimum contact angles are typically near 50°, and as such, substrate surfaces are often chemically treated to achieve this condition [51, 52]. The velocity at which the meniscus is dragged over the surface must also be optimized to achieve high rates of assembly, while avoiding the detrimental flows caused by excessive velocities that result in the recirculation of nanoparticles away from the accumulation zone [52]. High-yield capillary assembly is typically carried out at velocities of a few micrometers per second.

2.1.2. Trap design. Crucial to the assembly process is the fabrication of lithographically-defined trapping sites that are specifically designed to guide and position nanostructures derived from a colloidal synthesis offering a monodisperse collection of structures of known dimension. Suitably designed traps can capture individual nanostructures or a collection of structures arranged in well-defined patterns. In the absence of topographical traps (or substrate surface defects) a receding meniscus is able to effectively drag nanostructures across a planar surface leaving a bare substrate in its wake. If a trap is encountered, then the meniscus becomes distorted and pinned as a well-positioned nanostructure enters the trap due to the downward pointing component of the capillary force [45]. Continued evaporation causes the meniscus to be become depinned. If, at this point, the trap offers sufficient resistance (i.e., an energy barrier) to maintain the nanostructure within the trap, then the assembly has proven successful. The drying of residual liquid can, however, still maneuver the particle within the confines of the trap [56, 57]. Traps large enough to accommodate multiple particles assemble in much the same manner, but where particle-particle interactions can either augment the assembly process through interactions that bring nearby particles into close proximity or disrupt it through interactions that liberate previously trapped particles [13, 45]. Traps designed to capture spherical particles should be geometrically tailored to accommodate the desired particle or group of particles. Traps at the single particle level require lateral dimensions sufficient to house, not only the metal nanoparticle, but also any surface ligands or electrical double layers that envelop it [58]. Traps that are too wide capture multiple particles. Traps specifically designed to house multiple particles must take into account all of the aforementioned requirements as well as present a geometry that leads to the desired positioning of nanoparticles within the trap. Channel-shaped traps can lead to the assembly of dimers, trimers, or extended rows of nanostructures [13, 52, 58–60] while intricately shaped traps can give rise to more complex arrangements [13, 61]. Traps must be deep enough to pin the meniscus, bring about the downward pointing capillary force required for trapping, and provide resilience to removal as the meniscus recedes [45]. While deep traps give rise to the highest yield, deeply embedded particles can have reduced functionality and are undesirable when used in combination with contact printing (*vide infra*) [55, 62]. Well-designed traps typically have the upper half of the assembled structure protrude above the surface of the substrate.

2.2. Capillary assembly of complex colloids

Advancing capillary assembly techniques beyond spherical geometries into the realm of asymmetric nanostructures provides access to a set of physicochemical properties that are far more sophisticated, but where this opportunity is met with the challenges associated with a decidedly more complex assembly process. If nanostructure asymmetries are to be fully exploited, then patterned recesses must trap structures while simultaneously exerting control over their orientation within the trap. The assembly of nanorods, for example, requires a trap geometry that is different for structures aligned in an end-to-end as opposed to a side-by-side configuration, where it should be recognized that the capillary forces exerted depend upon whether the nanorod is parallel or perpendicular to the receding contact line [52]. Such challenges have now been met by a number of research groups as is demonstrated by the successful capillary assembly of single element nanorods [52, 53, 62–66], nanocubes [52, 55], and nanoprisms [54] as well as more complex architectures featuring concave facets [54] and nanowire geometries comprised of two alternating metal segments [56]. This section highlights these successes, provides an understanding of how the accumulation zone and trap design are influenced by nanostructure complexity, and describes post-assembly processes that have been used to enhance the functionality of the assembled structures.

2.2.1. Accumulation zone for complex structures. Populating the accumulation zone with asymmetric nanostructures introduces a number of complicating factors into the assembly process. Colloids of complex structures inevitably display greater levels of size and shape dispersity. Syntheses that generate such structures employ a wide range of facet-selective capping agents that promote anisotropic growth modes and stabilize the structures against agglomeration. These agents, however, do not necessarily meet the more severe demands of the capillary assembly process as they must resist agglomeration when placed in the much closer confines of an accumulation zone. Moreover, their interaction with the substrate material, especially if it is repulsive, can hinder assembly [55]. Such interactions are not well-characterized or understood. Cetyl trimethylammonium bromide (CTAB) has proven to be the most effective

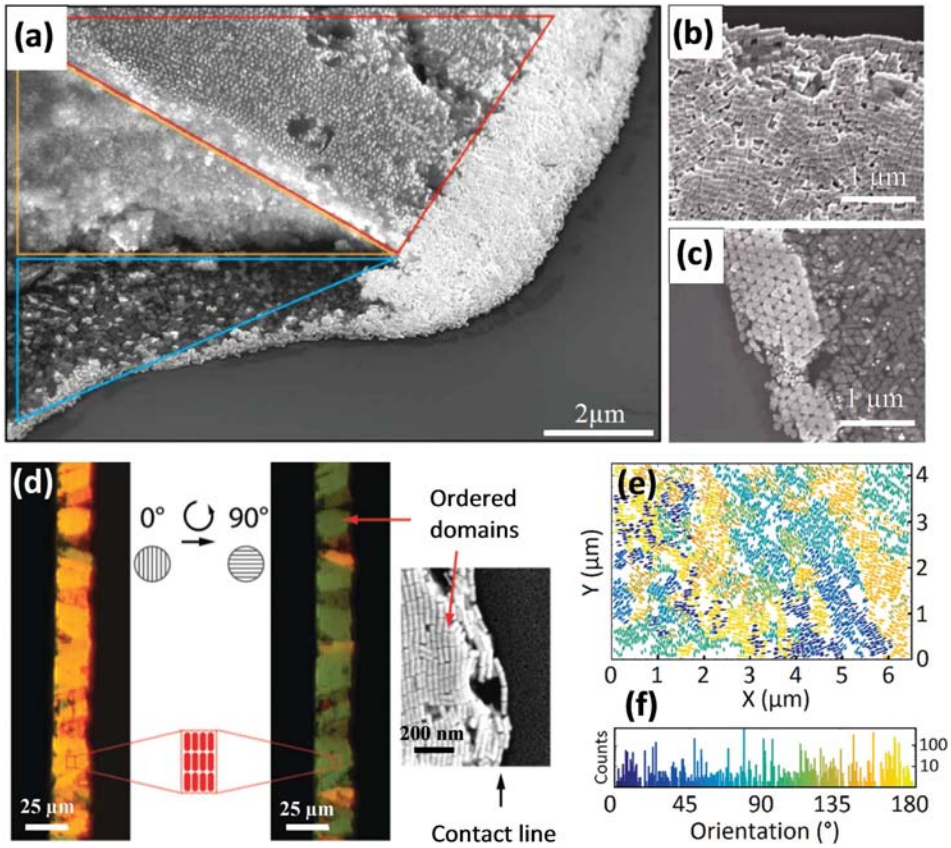

Figure 2. SEM images of dried accumulation zones comprised of (a) nanorods, (b) nanocubes, and (c) nanoprisms. The triangular frames in figure 2(a) denote the upper surface of the accumulation zone (red), its bulk interior (orange), and layers formed close to the substrate surface (blue). (d) Optical images of the accumulation zone where the light is polarized parallel (left) and perpendicular (right) to the contact line. The observed optical anisotropy indicates domain formation where nanorods preferentially align parallel to the contact line. (e) Maps of nanorod orientation for the monolayer adjacent to the substrate surface and (f) their corresponding angular distribution. (2a, e, f reproduced with permission from [52]. Copyright 2017 Macmillan Publishers Ltd.) (2b, c reproduced with permission from [54]. Copyright 2014 American Chemical Society.) (2d reproduced with permission from [53]. Copyright 2012 Wiley.)

surface ligand for colloidal assembly of complex structures to an extent that it has been used almost exclusively. Procedures are, however, often put in place to supplement existing quantities [53] or to add it when no ligand is present on the nanostructure surface [56]. The effectiveness of this surfactant molecule in stabilizing the dense colloid formed in the accumulation zone is attributed to the formation of a self-assembled bilayer on the nanostructure surface that presents an electrical double layer to adjacent structures [53, 67].

Strong spatial confinement within the accumulation zone has been demonstrated for nanorods [52, 53, 63], nanocubes [54], and nanoprisms [54, 68]. Figures 2(a)–(c) show SEM images of the accumulation zone formed for these three architectures after the solvent has dried. Such images reveal the complexity of accumulation zones when occupied with asymmetric nanostructures. They show that the structures contained within these zones display a significant degree of order with respect to each other and relative to the contact line. Well-studied is the organization of Au nanorods within the accumulation zone because order can be observed, not merely through SEM imaging on dried zones, but through the real-time optical monitoring of the polarization dependent optical response [53]. Nanorods are especially amenable to this *in situ* monitoring tool because light polarized along the length of the nanorod shows an LSPR that is distinct from that displayed by light polarized along its width (figure 2(d)). Together these morphological (figure 2(a)) and optical probes (figure 2(d)) indicate that the densification of the accumulation zone is accompanied by the formation of ordered domains where nanorods within the domain display smectic order. The domains, which can consist of thousands of nanorods, show preferential alignment such that there exists a strong tendency for the long axis of the nanorod to align parallel to the receding contact line. Nanorods situated at the leading edge of the meniscus display an even greater propensity for parallel alignment. In a recent study, it was demonstrated that a dried accumulation zone can be pealed from the substrate surface, making the nanorods in direct contact with the substrate accessible to SEM imaging [52]. An orientational analysis of the bottom monolayer (figures 2(e) and (f)) revealed that the long-range ordering exhibited by the bulk of the accumulation zone does not extend to the substrate surface. Here, nanorods display only short-range order (figure 2(e)) where the tendency toward

alignment with the contact line is absent (figure 2(f)), features that prove quite beneficial to the assembly process (*vide infra*).

2.2.2. Trap design for complex structures. The earliest example of capillary assembly able to capture asymmetric nanostructures in periodic arrays was that of Kuemin *et al* [63] who demonstrated that Au nanorods could be captured in reasonably high yield by traps with circular openings. While representing an obvious breakthrough, the assembly process was unsatisfactory from the standpoint that no control was exerted over the alignment of the nanorods within individual traps. Their follow-up study demonstrated that control could indeed be exerted over nanorod alignment and orientation relative to the receding contact line through the design of elongated traps that are only able to physically accommodate nanorods when their long axis is approximately parallel to the long access of the trap [53]. Accordingly, long narrow channels are able to direct the assembly of nanorod chains organized in an end-to-end configuration over micrometer-scale distances [62, 65, 66]. Other studies demonstrated that the preferential alignment of nanoprisms [54] and nanocubes [52, 54] could also be controlled by tailoring the trap geometry in all three dimensions.

With the trapping performance of nanorods within elongated traps being dependent on achieving alignment, it was understood that the likelihood of a nanorod being accepted into any given trap would diminish over that observed for spherical nanoparticles. The preferential alignment of nanorods parallel to the receding edge of the contact line (figure 2(d)), however, provided a mechanism for achieving high yield trapping using similarly aligned traps [53]. The authors were, however, surprised and somewhat perplexed by the fact that high yield trapping could also be achieved for perpendicularly aligned traps. A plausible explanation was provided by the subsequent study showing that the interface between the accumulation zone and substrate was characterized by nanorods with near-random in-plane alignment (figure 2(f)) [52] as it provided a mechanism for traps of any orientation to encounter similarly aligned nanorods. This explanation, however, required that nanorod insertion into the trap occur prior to its contact with the leading edge of the meniscus. This new understanding is consistent with increased yields occurring for a more densified and elongated accumulation zone [53, 62].

Trap design and its influence on the assembly process was markedly advanced in a recent study by Flauraud *et al* [52] in which they compared the nanorod trapping performance of standard elongated traps with that obtained using more complex designs. In doing so, they identified three distinct stages in the capillary assembly process: (i) the insertion of the nanorod into the trap, (ii) the trap providing resilience against nanorod removal as it encounters the receding meniscus, and (iii) the displacement of the nanorod within the trap by the capillary forces exerted as any residual solvent dries. Figure 3(a) shows a schematic of a captured nanorod within a standard straight-edged trap, a SEM image of the trapped nanorods, and an analysis of the trapping efficiency as a function of trap width and depth. The data shows that the trapping yield is compromised as the dimensions of the trap approach those of the ligand-encircled nanorod. Widths promoting high yields, however, suffer from the angular offsets observed in the SEM image. Increasing the depth of the trap results in higher yields because it offers greater resilience to nanorod removal. Such results mirror those of earlier parametric studies of the capillary assembly process [53, 62].

Many of the deficiencies of the straight-edged trap were overcome by using a funnel-shaped trap featuring a tapered recess that guides the nanorod into its final position (figure 3(b)). The near-elimination of the angular offset is accompanied by a trapping efficiency that increased more than 6-fold for 50 nm wide traps aligned parallel to the contact line. The most interesting aspect of their study, however, are the results obtained using a standard elongated trap with an adjacent auxiliary sidewall lithographically patterned from a hydrogen silsesquioxane layer (figure 3(c)). This symmetry-breaking structure leads to improved trapping, a higher resiliency to removal, and a nanorod that is consistently drawn to the sidewall feature regardless of whether it is placed on either side of the trap or even at its narrow ends. From a mechanistic standpoint, this feature acts to bias the post-insertion solvent evaporation that is responsible for the final positioning of the nanorod within the trap. The result is consistent with other studies showing the selective placement of nanostructures within a trap [56, 57, 66] or cases where one trapped structure is drawn toward another [54, 62]. By further increasing the complexity of the auxiliary sidewall the authors demonstrated that they could gain nanometer-scale control over the spacing between two nanorods aligned in an end-to-end fashion (figure 3(d)). This discovery is of the utmost significance because it provides the means by which nanoscale positioning can be exerted over a nanostructure within a trap having dimensions significantly larger than the captured structure, albeit with far greater demands placed on the required lithographic capabilities.

Additional capabilities have been demonstrated using increasingly sophisticated trap designs. Flauraud *et al* [52], for example, were able to manipulate the orientation of captured nanocubes within a trap. Using the same funnel-shaped traps described in figure 3(b), they were able to capture side-by-side nanocubes with their (100) faces in contact, but where the [110] axis was perpendicular to the substrate surface. Then through modifications to the trap design they were able to reorient identical nanocubes such that they displayed in-plane corner-to-corner alignment with their [111] axis normal to the substrate. Greybush *et al* [69] designed intricately shaped traps with two mutually exclusive regions in which one was designed to capture a Au nanorod while the other could only except a hexagonally-shaped upconversion nanophosphor ($NaYF_4$: Yb^{3+}, Er^{3+}). The close proximity of the two structures led to a several-fold increase in the achievable luminescence from the phosphor when

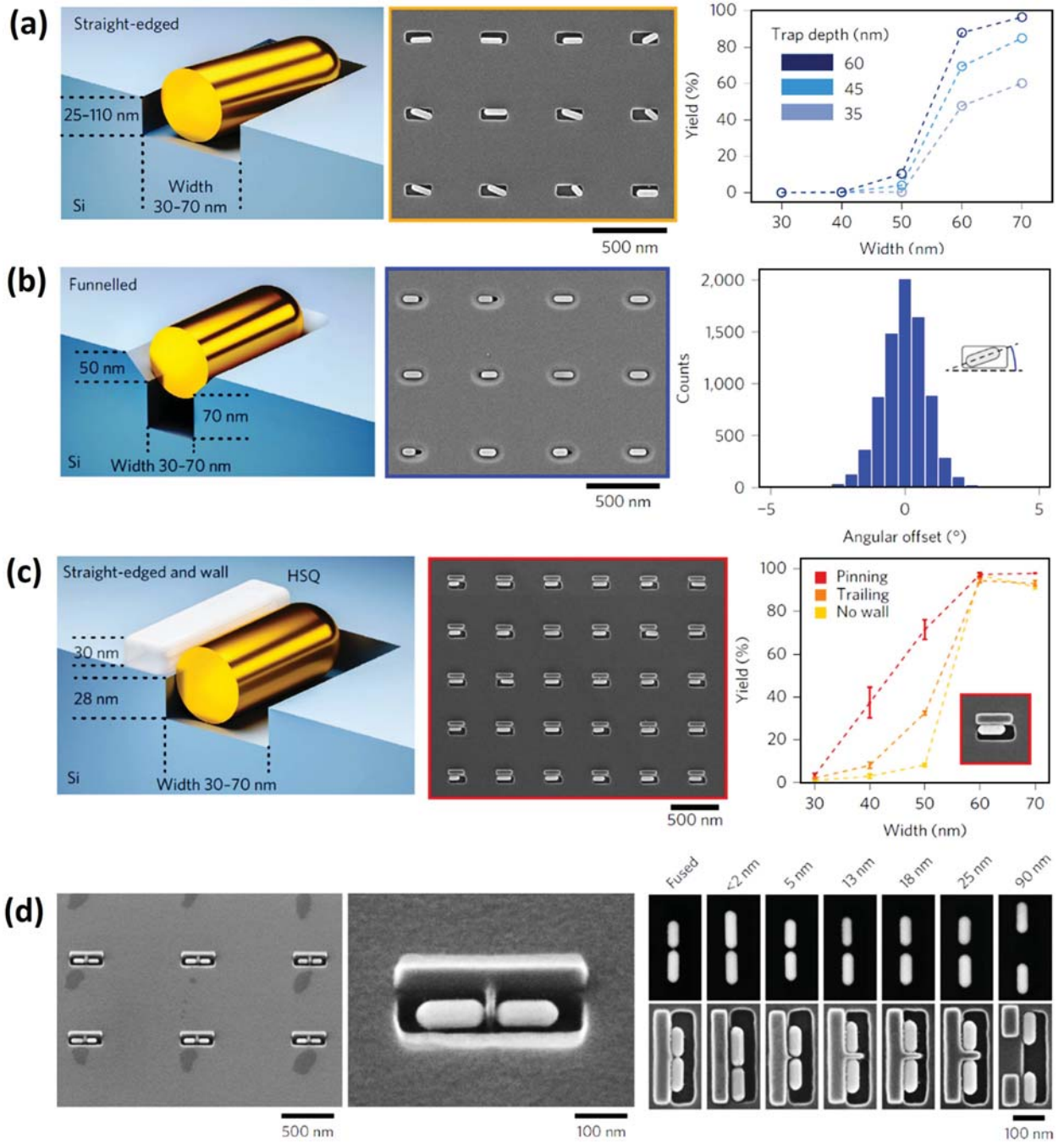

Figure 3. Schematics, SEM images, and a statistical analysis of the trapping performance for traps having (a) straight-edged sidewalls, (b) tapered sidewalls, and (c) an auxiliary sidewall. (d) SEM images demonstrating the nanoscale control achievable in the spacing between two end-to-end aligned nanorods positioned using the biasing capability of auxiliary sidewalls. (Reproduced with permission from [52]. Copyright 2017 Macmillan Publishers Ltd.)

exposed to the near-fields of a resonantly excited nanorod. Zhou *et al* [54] showed that an accumulation zone populated with both nanoprisms and spherical nanostructures, when exposed to suitably designed traps, captured only the nanoprisms. The nanospheres, which showed no resilience to removal from the traps, were carried away by the receding contact line. This demonstration is of potential significance because it provides the means to eliminate undesirable structures contained within the colloid from the assembly process. In the same study, they also demonstrated trap designs able to capture two nanoprisms in a bowtie configuration.

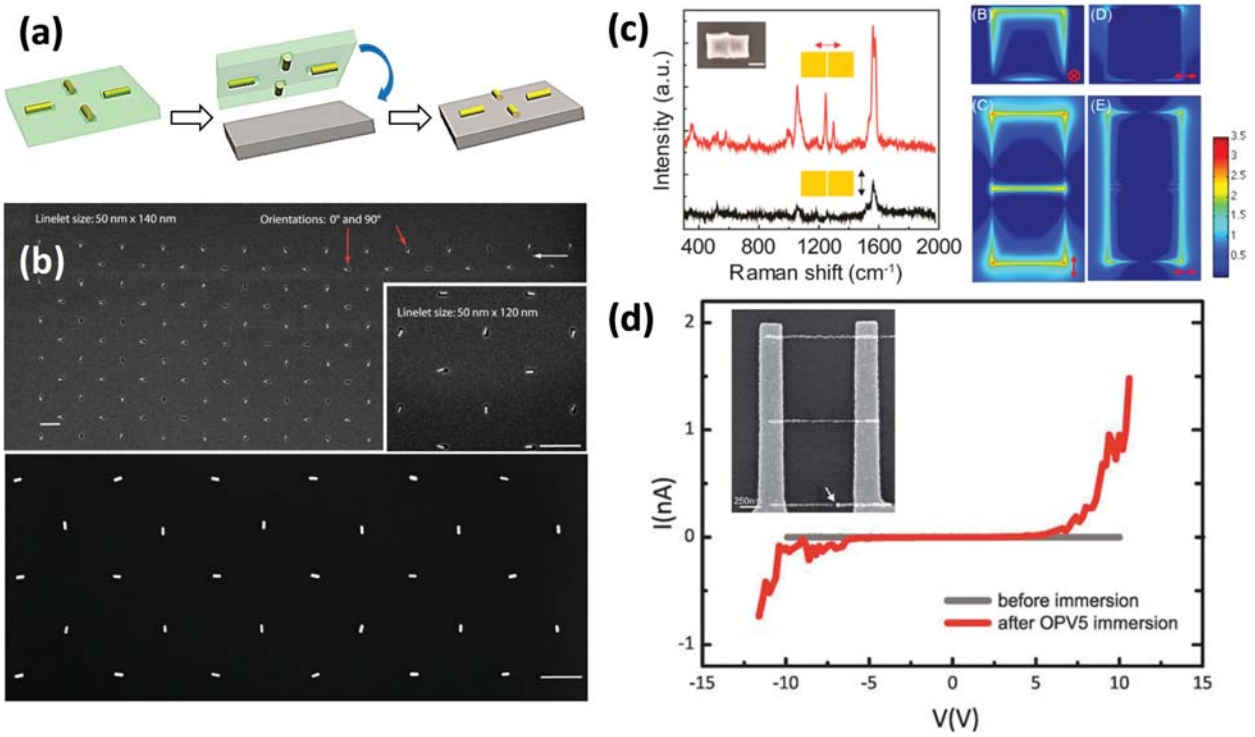

Figure 4. (a) Schematic of the microcontact printing process. (b) SEM images showing a capillary assembled surface of arrayed nanorods and the same pattern obtained on a Si substrate using the printing procedure. (c) SERS spectra from a Au nanocube dimer with concave facets functionalized with 1, 4–benzenedithiol (1, 4–BDT) for light polarized along the longitudinal and transverse directions and FDTD simulations of the plasmonic near-fields. (d) SEM image (inset) and *I–V* characteristics of a linear chain of Au nanorods extending across two contact pads for bare nanorods (grey curve) and ones that been functionalized with OPV-5 (red). (4b reproduced with permission from [53]. Copyright 2012 Wiley.) (4c reproduced with permission from [54]. Copyright 2014 American Chemical Society.) (4d reproduced with permission from [62]. Copyright 2013 Royal Society of Chemistry.)

2.3. Enhancing functionality through post-assembly processes

The application of post-assembly processes provides the opportunity to increase the functionality of capillary assembled surfaces. While demonstrations of capillary assembly using hard templates exist, most of the work carried out to date utilizes soft-template materials into which nanoscale patterns are imprinted using a reusable silicon stamp with nanoscale features defined by e-beam lithography. If the potential of these plasmonic nanostructures are to be fully realized, then it is imperative that the assembled arrays be transferable to a wide range of substrate materials in a manner that (i) preserves nanoscale gaps between adjacent structures, (ii) allows for a coupled response with the underlying substrate material, and (iii) can be integrated into Si wafer-based technologies. This section describes the progress made in meeting these processing challenges.

2.3.1. Microcontact printing. Microcontact printing provides a well-established processing technique for transferring nanostructures trapped in the recesses of a soft template to a planar substrate [55]. In this process, the product of capillary assembly is used as a stamp that is applied to a planar substrate material (figure 4(a)). In a typical procedure (i) a PDMS (polydimethylsiloxane) adhesion layer is applied to the target substrate, (ii) this substrate is then placed in contact with an inverted capillary assembled surface, (iii) temperature and pressure are then applied to the sandwich structure, (iv) the structure is then cooled, the pressure is released, and the transferred pattern is exposed, and (v) the PDMS layer is removed using an oxygen plasma. For high yield pattern transfer to occur, the capillary assembled nanostructures must protrude significantly from the patterned recesses in order to establish adequate bonding with the adhesion layer. This requirement is at odds with a capillary assembly process that realizes higher yields for traps of greater depth. Nevertheless, numerous groups have managed to balance these tradeoffs to achieve printed patterns of complex nanostructures [53–56, 62, 65] on substrate materials offering both greater technological relevance and a planar surface that provides a more conventional platform for fabricating device architectures. Figure 4(b) shows SEM images of capillary assembled nanorods before and after microcontact printing onto a silicon substrate [53].

The success of microcontact printing as an important post-processing procedure for capillary assembled structures has been demonstrated through application. Figure 4(c) shows surface enhanced Raman spectroscopy (SERS) data for microcontact printed nanocube dimers expressing concave facets that have been functionalized with 1,4–benzenedithiol (1, 4–BDT) as well as finite-difference time domain simulations of the plasmonic near-fields expected for a

nanocube dimer [54]. The data shows that a significantly enhanced SERS signal is achievable when light is polarized along the longitudinal axis of the dimer structure. In an impressive demonstration, Rey *et al* [62] transferred rows of Au nanorods across lithographically-defined contact pads. The oxygen plasma used to remove the adhesion layer also removed the CTAB molecules from the surface of the nanorods, leaving them isolated and separated by 6 nm gaps. The current–voltage (I–V) characteristics of the chains were then measured before and after functionalization with oligophenylenevinylene (OPV-5), a molecule known for its electron transport capabilities (figure 4(d)). While the gap between the nanorods resulted in an open circuit, the functionalized rods showed I–V characteristics synonymous with a tunneling effect.

Replicating a capillary assembled surface when there exists nanometer-scale gaps between adjacent structures can prove challenging using the microcontact printing method. Zhou *et al* [56], however, demonstrated a procedure that is capable of generating end-to-end aligned Au nanorods with a highly tunable and predetermined gap spacing. They first synthesized Au–Ni–Au multisegmented nanowires in the pores of an AAO template. They then etched away the template, functionalized the nanowires with CTAB, and carried out the capillary assembly procedure. The multi-segmented nanowires were then microcontact printed onto a SiO_2 substrate. In the final step, the Ni segment was selectively etched, dividing a single structure into two Au nanorods separated by a gap with a width equal to the length of the initial Ni segment. By adjusting the width of the Ni segment they could produce nanogaps of the desired dimension. Holzner *et al* [64], in an attempt to overcome the limitations of microcontact printing, devised an alternate procedure in which they spin coated a temperature sensitive polymer onto a target substrate, patterned recesses into it, and then trapped nanorods using capillary assembly. Then, instead of using the microcontact printing technique, they used elevated temperatures to sublimate away the polymer, leaving the assembled structures resting on the surface of the target substrate in a near-identical pattern.

2.4. Assembly of complex colloids using chemically nanopatterned substrates

The nanoscale building blocks accessible through colloidal suspensions can also be arranged into organized patterns using the electrostatic interactions originating from a substrate surface that has been chemically altered so as to present patterned areas that promote nanostructure adhesion while leaving the remaining surface devoid of nanostructures. The overall surface, therefore, presents a chemical contrast pattern that is characterized by alternating repulsive and attractive interactions between the two chemically distinct areas and the electrical double-layer/ligands that envelops colloidal structures. While this strategy has been widely used, the current discussion is limited to those studies that have fabricated chemical contrast patterns with nanoscale dimensions. Notable studies within this subset have demonstrated the capability

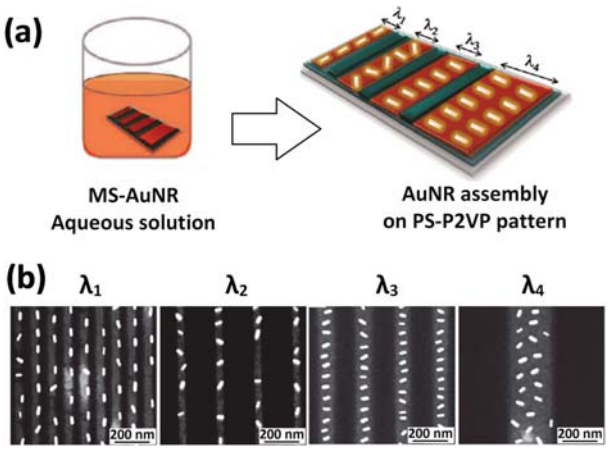

Figure 5. (a) Schematic showing a chemically nanopatterned surface with areas promoting (red) and inhibiting (green) nanorod attachment. (b) SEM images showing the nanorod patterns obtained as the width of the patterned strip (λ) is varied. (Reproduced with permission from [42]. Copyright 2012 American Chemical Society.)

of forming parallel rows of identical spherical nanoparticles [70, 71], nanorods [42], and trimers comprised of three nanospheres where each is of a different diameter [72].

As was the case for capillary assembly, the adaptation of the strategy to nanorods came with the challenge of aligning these asymmetric structures. To achieve this capability, the attractive interaction cannot merely respond in a hit-and-stick fashion, but must prove pliable enough to allow the nanorod to reorient after attachment. At the same time, the attractive forces must be strong enough to inhibit nanorod dissociation. Nepal *et al* [42] have overcome these challenges to form organized rows of nanorods. The devised process directed the assembly of Au nanorods using a chemical contrast pattern comprised of polystyrene (PS) mats and poly-2-vinylpyridine (P2VP) brushes (figure 5(a)). By systematically reducing the width of the P2VP strips they were able to disrupt the balance of nanorod interactions with the (i) patterned strip, (ii) the adjacent chemical boundary, and (iii) neighboring nanorods to an extent that it first led to a reduction in the number of nanorod rows from two to one and then to a transformation in nanorod alignment from a side-by-side to an end-to-end configuration (figure 5(b)). Further disruptions to the electrical double-layer caused by the addition of NaCl to the colloid led to a densification of the nanorod packing, a result consistent with earlier work performed on spherical nanostructures [73].

3. Templated dewetting

Ultrathin metal films, when exposed to elevated temperatures, tend to reorganize into nanoscale droplets through a process referred to as dewetting. It, in many ways, represents the vapor phase analog to colloidal syntheses in that it provides a straightforward strategy for forming crystalline nanomaterials. The dewetting process, which has been extensively reviewed [35–39], is driven by an energy minimization of the

film–substrate system as it pertains to the metal–substrate interfacial energy as well as the surface-free energy of both the metal and the exposed substrate. It is, in essence, energetically favorable for a continuous metal film with a high surface-free energy to reorganize into three-dimensional droplets so as to reduce its overall surface-to-volume ratio, a reorganization that is done at the expense of partially exposing a substrate with a low surface-free energy. Dewetting can occur for films in either the liquid- or solid-state, but where each has mechanistically distinct aspects. In particular, the mass transport required for solid-state dewetting is primarily achieved through the directional surface diffusion of atoms, whereas liquid-state dewetting includes a sizeable bulk diffusion component. This difference allows for solid-state dewetting to occur at temperatures well below the melting point, but where the overall process occurs at a much slower rate. While the vast majority of dewetting studies have been carried out using standard laboratory furnaces, alternative methods for inducing the dewetting phenomenon require the use of a laser [74–79], ion [80], or electron [81] beam. Here, focus is placed on solid-state dewetting carried out using standard practices.

The solid-state dewetting of polycrystalline films is a highly complex process influenced by the film thickness [82], temperature [39], grain boundaries [83], faceting [84], strain [36], the crystallographic orientation of the substrate [85], surface reconstructions [86, 87], and interface chemistry [88]. While an in-depth understanding is outside the scope of this review, its key elements are of significance. A metal film deposited at room temperature exists in a thermodynamically unfavorable state, but where the constituent atoms lack the kinetic energy required to reorganize into a more favorable state (i.e., the energy needed to dewet). With sufficient heating, this limitation is lifted for atoms residing on the surface (which have a much higher mobility than those confined in the bulk). The dewetting process is initiated when these surface diffusion processes result in the nucleation of holes in the film that extend to the substrate surface. Such holes can originate at grain boundary triple junctions [39], high angle grain boundaries [83], or defects [39]. Once formed, the film becomes destabilized by capillary driven solid-state diffusion away from the film–substrate edges, a process that sees more and more atoms near the edge exposed to the surface as it retracts and the adjacent rim thickens. Continued dewetting gives rise to Rayleigh-like instabilities [89], fingering instabilities [90] and the intersection of retracting edges from multiple dewetting fronts, all of which eventually lead to the formation of isolated islands. Continued diffusion advances the island shape toward its equilibrium configuration, which for an fcc metal is a substrate-truncated Wulff shape [91] (i.e., a truncated octahedron expressing six square {100} facets and eight hexagonal {111} facets).

While solid-state dewetting offers a straightforward fabrication route for substrate-supported metal nanostructures, it is disadvantageous in that there is a lack of control over nanoparticle size, spacing, and placement [82]. Lithography, however, provides the means to transform this disorganized self-assembly process into a directed assembly technique where control is exerted over these key parameters. The overall strategy is one where lithographically-defined features are used to activate the dewetting phenomenon in a manner that, not only overrides natural tendencies, but which forces the assembly to occur in a highly deterministic manner. The role of lithography is, hence, to establish preprogrammed target sites for the agglomeration of single-crystal nanostructures from set quantities of material. These so-called templated dewetting techniques are well-established for single element nanostructures with near-spherical geometries. Here, we present these techniques and describe early efforts being forwarded to adapt them to the assembly of more complex nanostructures.

3.1. Templated dewetting through film patterning

Lithography provides the means to subdivide an otherwise continuous metal film into smaller units through (i) the deposition of a film followed by the selective removal of unwanted areas using wet or dry etching techniques or (ii) the deposition of a film through openings in a patterned photoresist followed by the removal of the unwanted metal and photoresist (i.e., lift-off). Features defined in this manner display edges that, when exposed to elevated temperatures, retract in manner similar to those associated with the randomly formed holes that develop in the early stages of dewetting and which are a prerequisite for dewetting to occur. These lithographic features can, hence, replace the random instabilities resulting from spontaneous hole formation with programmable instabilities. In doing so, the dewetting process can be manipulated to evolve in an organized manner. It should nevertheless be recognized that random instabilities can still occur and will corrupt pattern formation if the assembly process is carried out on the time- and length-scales that allow for their emergence. In the earliest demonstration of this templated dewetting technique, Kim *et al* [92] lithographically-defined square and rectangular patterns in a polycrystalline film of Au that reproducibly assembled into organized patterns of near-spherical structures. This technique has notably been extended to fabricate similarly shaped nanostructures as periodic arrays [75] and in highly complex patterns using laser-induced dewetting [77–79]. A variation of this directed dewetting approach replaces lithographic patterning with shadow masks derived from patterns of self-assembled templates such as close packed PS spheres [93] or diblock copolymers [94], but where true long-range order is sacrificed.

Thus far, few examples exist where this fabrication scheme has been extended to what we term as complex nanostructures. The formation of alloys by dewetting bilayer films comprised of two miscible metals provides an obvious opportunity. To date, this technique has been exploited for continuous metal films [95–97], but not for patterned bilayers. We have, however, for the purpose of this review, formed periodic arrays of AuPd nanostructures using the templated dewetting technique shown schematically in figure 6(a). Nanoimprint lithography (NIL) was used to imprint a resist with a lithographically manufactured stamp comprised of a

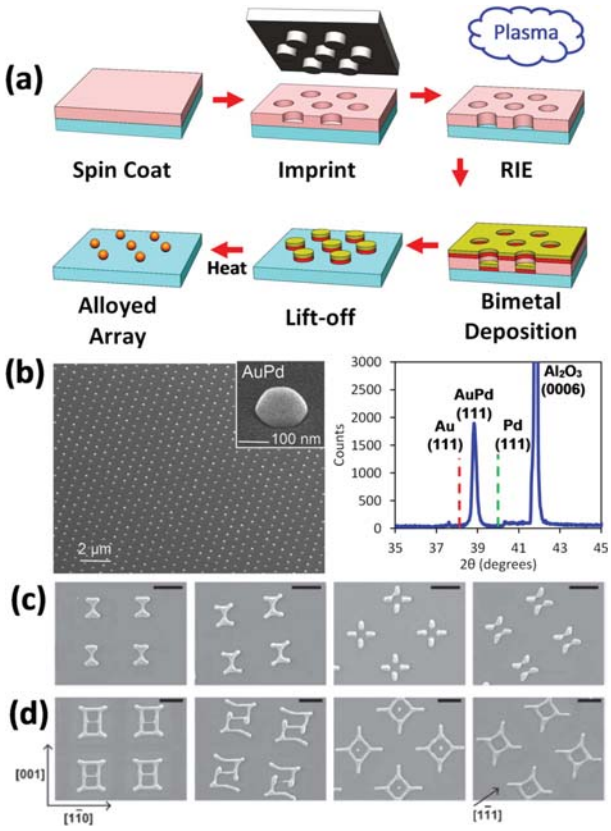

Figure 6. (a) Schematic of the templated dewetting process used to generate periodic arrays of $Au_{0.7}Pd_{0.3}$ nanostructures using a planar substrate. (b) SEM image of the AuPd array and x-ray data obtained after the assembly process. SEM images of the structures formed in the templated dewetting process using square patterns with edge lengths of (c) 12 μm and (d) 19.7 μm defined in a single-crystal film of [110]-oriented Ni. The in-plane crystallographic directions of the Ni film relative to the pattern orientation are shown on figure 6(d) (scale bar = 10 μm). (6c, d reproduced with permission from [101]. Copyright 2011 Wiley.)

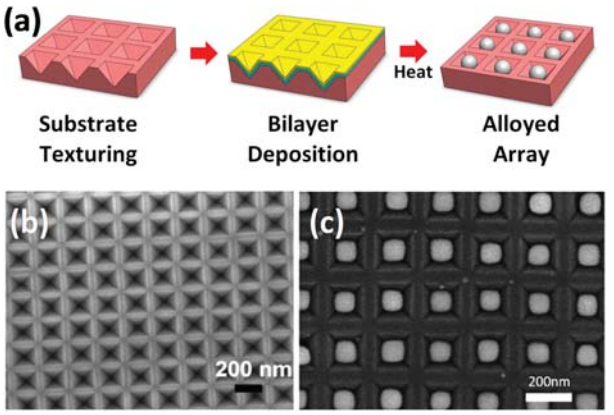

Figure 7. (a) Schematic of the templated dewetting process used to generate periodic arrays of CoPt nanoparticles using a textured substrate. SEM images of a (b) textured substrate and (c) the array of CoPt nanoparticles formed after the dewetting of a Co/Pt bilayer. (7b reproduced with permission from [107]. Copyright 2009 Wiley.) (7c reproduced with permission from [76]. Copyright 2013 Wiley.)

hexagonal array of pillars, after which a reactive ion etch was used to expose the substrate surface. A Au/Pd bilayer was then deposited followed by a lift-off procedure. When heated, the patterned areas formed a periodic array of nanostructures that have an x-ray diffraction signature corresponding to an alloy composition near $Au_{0.7}Pd_{0.3}$ (figure 6(b)). It is noted that immiscible and partially miscible systems provide the opportunity to form bimetallic nanostructures using this same methodology [98–100].

Thompson and co-workers have devised a related strategy that gives rise to dewetted structures with complex shapes [101]. The key difference is that they lithographically-defined patterns using single-crystal films (as opposed to polycrystalline) that are epitaxially aligned with a crystalline substrate. This difference leads to added control because (i) the disorderly influences that grain boundaries have on dewetting [83] are absent and (ii) the anisotropic dependence of edge retraction in different crystallographic directions provides an auxiliary control for directing the assembly process. Figures 6(c) and (d) show the intricate structures accessible when square patterns of two different edge lengths are first lithographically-defined from a single-crystal film of Ni and then exposed to a dewetting procedure [101]. For each case, the [110]-axis of Ni is normal to the substrate surface, but where the orientation of the square pattern relative to the various in-plane axes of the Ni film is varied. The fact that each pattern is reproducible, yet different, is representative of the anisotropies present. It is noted that Ye *et al* [102] recently carried out related work using [100]- and [110]-oriented Pd films. Interestingly, Rack *et al* [79] has achieved equally complex shapes in polycrystalline films using a pulsed laser dewetting technique that for short durations melts the Ni film. While the dimensions of all of these structures are quite large when compared to the other structures described in this review, the degree of sophistication is nevertheless impressive.

3.2. Templated dewetting through substrate patterning

A second approach to templated dewetting involves the deposition of a continuous metal film over a substrate surface that has been lithographically patterned, where the resulting surface topography is designed to create programmed instabilities at high curvature sites that cause the film to rupture when heated. These ruptures then act as the retracting edges from which the film dewets (figure 7(a)). From a mechanistic standpoint, the substrate texture introduces a curvature driven component into surface self-diffusion processes that leads to a net flux of atoms away from the high positive curvature regions (i.e., peaks and ridges). This flattening of the film results in an overall decrease in the free surface energy, but where the process is interrupted for sufficiently thin films when the flattening process exposes the underlying substrate. At this point, the continuous film is destabilized and the dewetting process prevails. This strategy, which was first demonstrated by Giermann and Thompson [89], has been used to assemble periodic arrays from films of Au [89, 103–105], Ag [106], Co [107] and Sn [108] where these demonstrations use either conventional or laser heating.

This work revealed that the success of the directed assembly process, for a given texture, is dependent upon the optimization of the film thickness; films that are too thin break up in a disorganized manner due to natural instabilities on length-scales smaller than those of the patterned features while those that are too thick form structures that are larger than and often incommensurate with the patterned features.

As was the case for templated dewetting through film patterning, the dewetting of metallic bilayers on textured substrates provides a relatively straightforward method for obtaining periodic arrays of alloyed nanostructures. Alloyed arrays of AuAg [109], CoPt [76] and AuNi [110] have been demonstrated using this strategy. Figures 7(b) and (c) show SEM images of a patterned substrate and the CoPt nanoparticles formed during the assembly process. Substrate texturing involved the use of a sacrificial silicon nitride layer into which square openings were defined using interference lithography. The exposed Si substrate was then treated with a KOH solution that anisotropically etches Si, resulting in an array of pits shaped as inverted pyramids with [111]-oriented sidewalls [107]. The remaining silicon nitride layer is then etched away and the Co/Pt bilayer is deposited and dewetted [76]. Interestingly, the authors compared the magnetic properties of CoPt nanostructures formed through conventional and laser dewetting using identical templates and found the conventional approach to be superior. It is noted, that a related approach has been widely used to fabricate arrays of nanostructures where the lithographically-defined substrate is replaced with textured surfaces of AAO [111, 112], anodic TiO_2 [35], close packed spheres [113, 114] and mechanically dimpled surfaces [74]. Such approaches have given rise to a range of complex nanostructures including alloys of AuAg [114], FePt [114, 115] and FePdCu [115].

3.3. Templated dewetting followed by post-assembly processes

As was the case for capillary assembly, templated dewetting also provides avenues for applying post-assembly processes. In this section, we describe a straightforward strategy that has been forwarded by our group in which arrays of Au nanostructures are first synthesized and then exposed to a high-temperature vapor-phase environment that transforms them into more complex structures [116–120]. Periodic arrays of Au nanostructures were fabricated using the process shown schematically in figure 8(a) in which a Au/Sb bilayer is deposited through a lithographically-defined shadow mask and then heated to high temperatures [41, 82, 121]. In this process Sb is used, not for the purpose of alloying, but as a sacrificial material that is beneficial to the directed assembly process. When the bilayer is heated, it results in (i) the formation of a thin AuSb eutectic surface layer and (ii) the preferential sublimation of Sb from the sides of the structure because the Au inhibits sublimation from the top surface. The net result is a greatly accelerated dewetting process brought on by the fast kinetics associated with a liquid overlayer and the advancement of sublimation fronts from all sides that drive the Au toward the center of the structure. In time, all of the Sb is lost to the vapor phase and a single Au nanoparticle is left resting on the substrate surface at each of the arrayed positions. The Au nanostructures formed using this method are single-crystals that show weak faceting consistent with a substrate-truncated Wulff shape (figure 8(b)). The advantage of this technique over those described in section 3.1 is that the agglomeration process is accelerated to such an extent that 100 nm nanostructures can be generated using a shadow mask with micrometer-scale features through which as little as a monolayer of Au is deposited, a trait that greatly diminishes the demands placed on lithographic processes.

Figure 8(c) shows a schematic of the procedure used to alter the shape and chemical make-up of the Au nanostructures. It involves the placement of a foil of a second material in close proximity to the arrayed nanostructures and then heating the sandwich structure to elevated temperatures. The directed assembly process that ensues sees the Au nanostructures act as heterogeneous templates for adatoms that are sourced from the foil through sublimation. Crucial to the process is that processing conditions be chosen to prohibit the spontaneous homogeneous nucleation of stable adatom clusters, so that the Au templates act as the only sites on the substrate where chemical and morphological transformations occur. Once the templates undergo the desired transformation the assembly process is terminated through cooling.

Figures 8(d)–(f) show SEM images of periodic arrays of complex nanostructures formed using three mechanistically distinct variations of the templated assembly process. In the first example, a Ag foil is used to source adatoms to Au templates to obtained alloyed AuAg structures with nanoprism-like morphologies [116]. The structures are [111]-oriented, exhibit four prominent (111)-facets, and are epitaxially aligned with the [0001]-oriented sapphire substrate in one of two in-plane orientations offset by 180°. From a mechanistic standpoint this high-temperature vapor-phase growth mode is highly unusual in that the morphology of the structure veers away from the equilibrium Wulff shape. This growth mode, which was predicted by Baletto *et al* [122] using molecular dynamics simulation, is instead dominated by kinetic processes that see (i) Ag adatoms arriving predominantly to the base of the Au structure via substrate surface diffusion, (iii) facet-dependent diffusion rates, and (iii) Ehrlich–Schwoebel barriers that inhibit adatom motion between facets [116]. Noteworthy, is that the same technique has since been used to generate similarly shaped AuCu structures [119]. The assembled nanoprisms have been demonstrated in hydrogen sensing [116], catalytic [119], and photocatalytic [119] applications.

In a second example, Sundar *et al* [117] replaced the foil with a Ge substrate and assembled Au/Ge heterostructures. This directed assembly route took advantage of both the deep eutectic that exists in the Au–Ge phase diagram ($T_E = 361$ °C) and the immiscibility that these two elements exhibit in the solid-state. The arrival of Ge to the Au template at temperatures well above T_E leads to the formation of a liquid AuGe alloy that when cooled below T_E phase separates into two immiscible components sharing a common interface. Selective etching of the Ge component reveals that the structures exhibit an

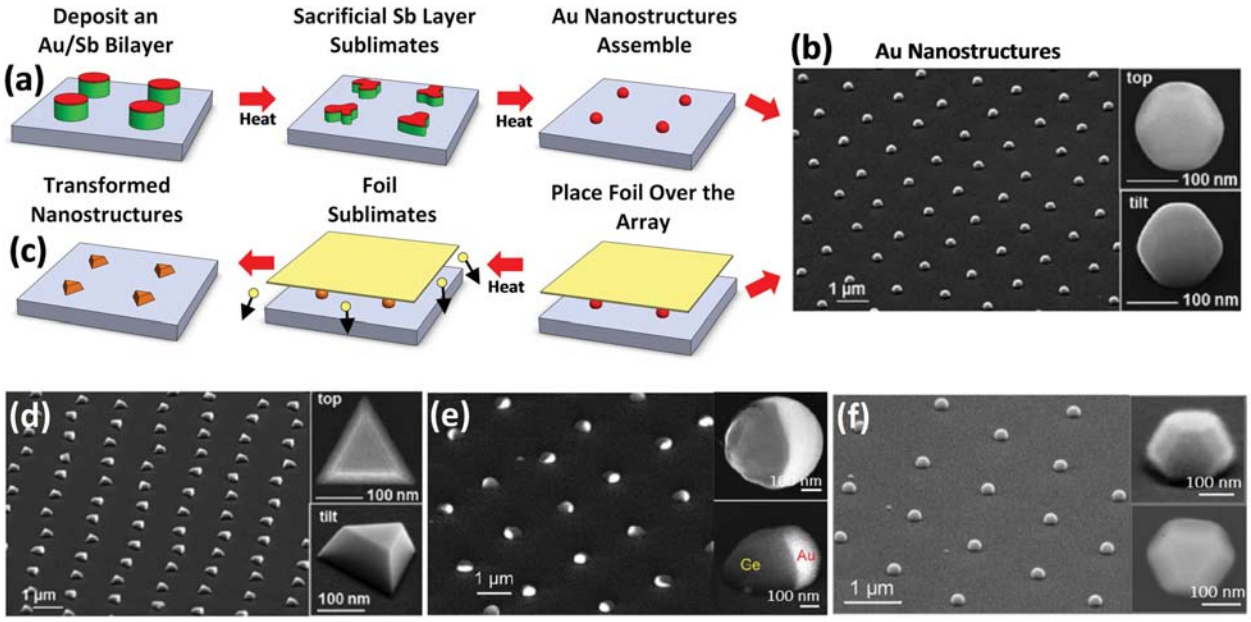

Figure 8. (a) Schematic of the procedure used to generate periodic arrays of Au nanostructures and (b) an SEM image of the structures formed. (c) Schematic of the procedure used to transform the Au nanostructures into more complex structures using high-temperature vapor-phase post-processing. SEM images of arrayed Au structures that have been transformed into (d) AuAg nanoprisms, (e) AuGe heterostructures, and (f) Wulff-shaped Pd nanostructures. (8b, d reproduced with permission from [116]. Copyright 2009 Royal Society of Chemistry 2015.) (8e reproduced with permission from [117]. Copyright 2014 Wiley.) (8f reproduced with permission from [118]. Copyright 2013 American Chemical Society.)

acorn-like morphology where a thin Au cap partially encapsulates the underlying Ge. These same etching experiments quite surprisingly revealed that the Ge blue-shifts the Au plasmon peak relative to the standalone Au structure.

In a third example, a Pd foil is placed in close proximity to the Au nanostructures and the temperature is raised to levels where Pd and Au are susceptible to sublimation and evaporation, respectively [118]. In such a scenario, the foil acts as both a source of Pd and a sink for evaporated Au while the Au template acts as a heterogeneous nucleation site that offers complete miscibility. Crucial, however, is the fact that the supply of Pd is essentially inexhaustible while the supply of Au is finite since any Au that diffuses into the foil is unlikely to reenter the process. The end-result is a time-dependent directed assembly process that sees the Au templates transform from pure Au, to a AuPd alloy with increasingly higher levels of Pd, and then finally to a strongly faceted Wulff-shaped Pd nanostructure, where any of the intermediate compositions can be obtained by terminating the assembly process at the appropriate time through rapid cooling. The overall process can be characterized as having sacrificial Au templates that temporarily act as heterogeneous nucleation sites for Pd prior to being consumed through evaporation.

4. Syntheses carried out at the liquid–substrate interface

Colloidal syntheses remain unrivaled in terms of generating complex nanostructures with a high degree of architectural and compositional complexity. While the aforementioned techniques involving the directed assembly of colloids have the potential to place such structures on substrates in an organized manner, they have not yet progressed to a stage where such capabilities are applicable to arbitrarily chosen nanostructures. An alternate strategy relies on practicing wet chemistry methods directly on the surface of a substrate where lithographically-defined features provide the controls needed to direct the reactions to a desired endpoint. One approach, which has been forwarded by the Mirkin group [123], sees the deposition of lithographically-defined droplet arrays where each droplet contains the precursors required to synthesize a single metallic nanoparticle from a spontaneously nucleated seed. A second approach, which has been forwarded by our group [41], practices seed-mediated colloidal syntheses on arrays of substrate-immobilized templates. In this section, these approaches are described as they relate to the synthesis of complex nanostructures.

4.1. Spontaneous nucleation of metallic nanostructures in attoliter-scale droplets

Scanning-probe techniques allow for the application of attoliter-scale droplets to hydrophobic substrate surfaces using nanometer-scale tips in combination with the programmed movements of a piezoelectric scanner. If each droplet contains the chemical precursors required for the solution-based synthesis of a single nanostructure, then under suitable processing conditions, the technique provides the means to form nanostructures at pre-specified surface sites. Such techniques,

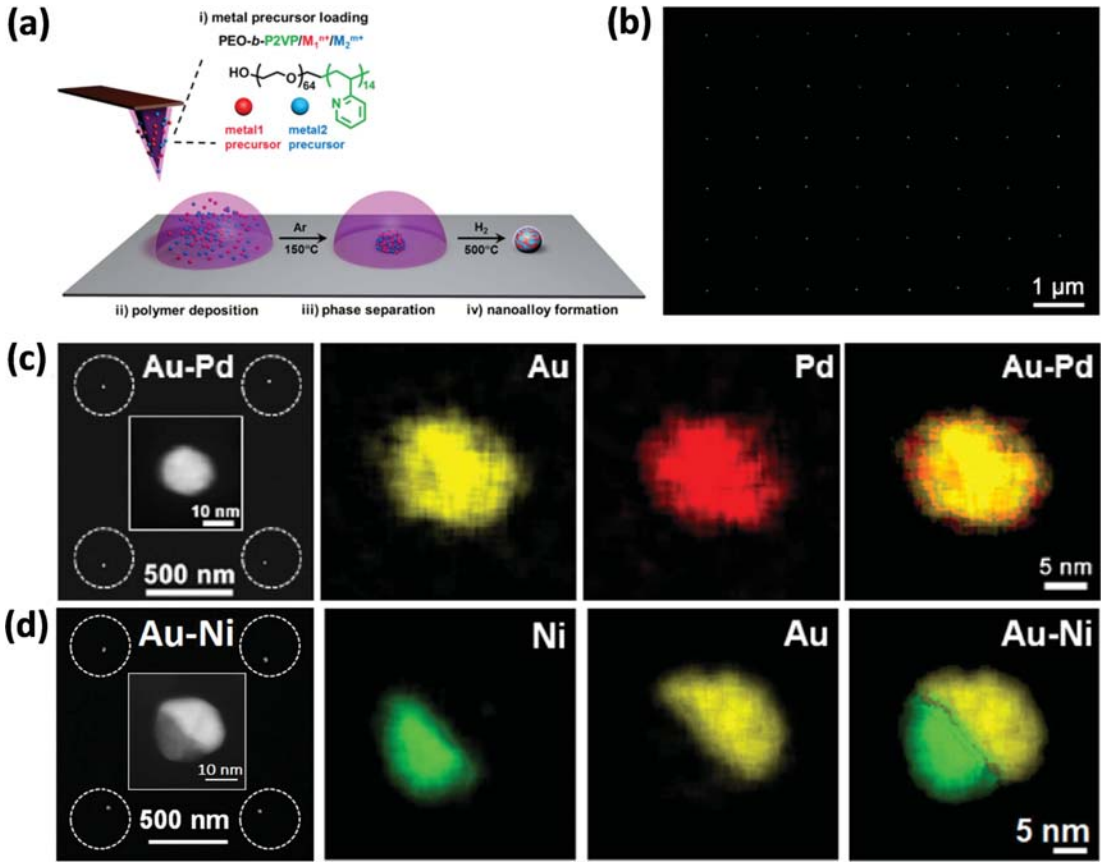

Figure 9. (a) Schematic of the scanning probe block copolymer lithography (SPBCL) process used to fabricate arrays of alloyed nanostructures. (b) SEM image of an array of AuPd nanoparticles. High-angle annular dark-field scanning transmission electron microscopy (HAADF–STEM) images and elemental mapping for (c) alloyed AuPd and (d) phase-segregated Au/Ni nanostructures. (Reproduced with permission from [123]. Copyright 2015 American Chemical Society.)

which fall under headings such as dip-pen nanolithography and polymer pen lithography [124, 125], use what is in essence a printing process to write, not nanostructures, but arrays of chemical reactors where each is able to facilitate the wet-chemistry required to synthesize a single nanostructure [40]. While a single tip is limited by the serial nature of the printing process, millions of structures can be printed per minute over large areas using the massively parallel capabilities brought about by tip arrays.

Figure 9(a) shows a schematic of the process used to form a metallic nanostructure at a well-defined position using tip-directed chemistry [123]. In this process, chemical precursors are first cast onto a probe that is then positioned over a target site. It is then momentarily brought into contact with the substrate surface where the dwell time and withdrawal speed play critical roles in determining the deposited volume. The role of the probe in the overall process is, hence, to establish the position in which a chemical reaction will occur and to transfer a well-defined volume of reactants to this position. The role of the deposited droplet is then to facilitate a chemical reaction and provide a confining boundary in which the reaction occurs. Reactions are typically initiated through the application of outside stimuli such as heat, an oxygen plasma, or light and must be carried out in a manner that gives rise to a single nucleation event that consumes all reactants before a second nucleation event occurs. Once the structure is formed, a high-temperature anneal is applied to (i) decompose and drive off all residual chemicals and (ii) promote nanostructure formation and crystallinity. Demonstrations of tip-directed assembly processes have been demonstrated for single-component nanostructures of Au, Ag, Pt, and Pd with near-spherical geometries [126–128]. The technique stands out for its ability to form nanostructures with sub-20 nm diameters. In fact, larger sizes are more problematic because reactants are present in individual droplets in quantities sufficient to promote multiple nucleation events.

Chen *et al* [123], using a technique referred to as scanning probe block copolymer lithography, have extended tip-directed assembly methods to the synthesis of numerous complex nanoparticles in the form of alloys and Janus structures. In their devised method, they form an aqueous solution containing a blend of multiple metal precursors (e.g., $HAuCl_4$ and Na_2PdCl_4) and a block copolymer. The metal precursors provide the source of metal ions needed to form the nanoparticle where the ratio of metal ions determines the nanoparticle composition. Attoliter droplets of the precursor are then deposited in arrays onto a substrate material. When heated to 150 °C, the block copolymer coordinates with the

metal ions to form a single structure on the substrate surface. Further heating to 500 °C in a H_2 atmosphere leads to the decomposition of all residual chemicals, forming a single-crystal nanostructure at each of the arrayed positions (figure 9(b)). In this manner, periodic arrays of numerous binary alloys comprised of combinations of Au, Ag, Pd, Ni, Co, and Pt have been synthesized along with a ternary alloy of Au, Ag and Pd. Elemental mapping of the structures indicate alloy formation (figure 9(c)) for all combinations except Au–Ni, which formed a phase-segregated Janus structure (figure 9(d)) due to the immiscibility of these two elements at the anneal temperature.

4.2. Template-mediated syntheses performed at the liquid–substrate interface

Heretofore, this review has primarily focused on techniques that are capable of fabricating periodic arrays of substrate-immobilized nanostructures on bare substrates. There is, however, the opportunity to further process existing arrays such that the complexity of the nanostructures is enhanced. The most viable means of achieving this outcome is through the adaptation of template-mediated colloidal protocols to the substrate-based platform by treating arrayed structures as templates in syntheses employing wet-chemistry. This strategy, which has been the subject of a prior review [41], hence, offers increased synthetic capabilities to any of the techniques previously described in this review. This section summarizes the progress made to date, where the subject is subdivided into syntheses utilizing (i) reactions that reduce aqueous metal ions onto arrayed templates and (ii) galvanic replacement, dealloying, and etching reactions that remove some of the templated material.

4.2.1. Template-mediated synthesis through heteroeptiaxial deposition. The reduction of aqueous metal ions onto preexisting structures (i.e., the template) provides a straightforward means for transforming single-component metal nanostructures into multicomponent systems characterized by sharp interfaces displaying a heteroepitaxial relationship. Through the application of suitable chemical controls, the starting template material can be transformed into a Janus structure, a core–shell structure, or more complex architectures where the starting template becomes partially encircled by a frame or decorated with multiple structures in an organized manner. As the initial structure is reconfigured, so too are its physicochemical properties, offering the opportunity for realizing novel behaviors, enhanced functionalities, and a high degree of tunability. While such synthetic pathways have been widely practiced using colloidal templates [19], only a few demonstrations exist where they have been practiced on arrays of substrate-immobilized templates [129–131]. These results, not only provide proof-of-principle demonstrations, but have also acted to highlight key differences between colloidal and substrate-based growth modes. Here, we describe the techniques adapted from colloidal chemistry to the substrate-based platform, summarize the unique features of this approach, and review the work carried out to date.

Template-mediated colloidal syntheses are able to achieve exacting controls over the shape and chemical make-up of bimetallic nanostructures [19, 132]. These reaction pathways typically exert control over heterogeneous depositions through the manipulation of reaction kinetics [133, 134] and/or the use of facet-selective capping agents [20, 135]. Reaction schemes dominated by kinetic factors realize shape-control by varying the rate at which metal ions are reduced onto the template, where a progression from fast to slow kinetics typically transforms the deposition process from conformal to asymmetric. Capping agents suppress the deposition of reduced metal ions onto facets where it is chemisorbed while allowing for nearly unobstructed deposition on other facets. If a facet-selective capping agent is available in excess during the deposition, then any newly formed facets of this type will also become protected. This inevitably leads to the transformation of multifaceted templates into structures dominated by a single facet-type. The schematic in figure 10(a) shows the expected transformation of Wulff-shaped Au templates into Au@Ag nanocubes when Ag^+ is reduced in the presence of a (100) capping agent.

The adaptation of synthetic protocols from solution-dispersed to substrate-immobilized templates fundamentally alters the nanostructure formation process and provides additional synthetic controls through which growth pathways can be manipulated. The templates available to substrate-based syntheses are no longer restricted to those that are generated through colloidal syntheses, since they can be derived from or subjected to vapor phase processing capable of enhancing crystallinity through high temperature anneals. Such seeds can present pristine surfaces unencumbered by stabilizing agents that can then be utilized as is or functionalized to meet the requirements of a specific growth mode. While the entire surface of the template is available for deposition in colloidal growth modes, the steric barrier provided by the substrate inhibits symmetric growth modes, a feature that lends itself to the formation of asymmetric structures even when otherwise symmetric growth modes are utilized [41, 136]. In no case is the template material enveloped by the depositing layer, instead becoming encapsulated by the substrate on its underside and by the metal overlayer elsewhere. Epitaxy provides the means to crystallographically orient the template material relative to the substrate material. This capability, in combination with the steric barrier offered by the substrate, allows for emergence of a unique nanostructure architecture for each template orientation even when exposed to identical synthetic procedures.

The first demonstration of the heterogeneous deposition in the liquid phase onto arrayed templates was carried out by Gilroy *et al* [129] using Au seeds formed in the vapor phase using the technique described in section 3.3 [121]. The synthesis performed was unique in that Ag^+ ions were reduced with ascorbic acid onto the Au seeds with pristine surfaces (i.e., surfaces without capping or stabilizing agents).

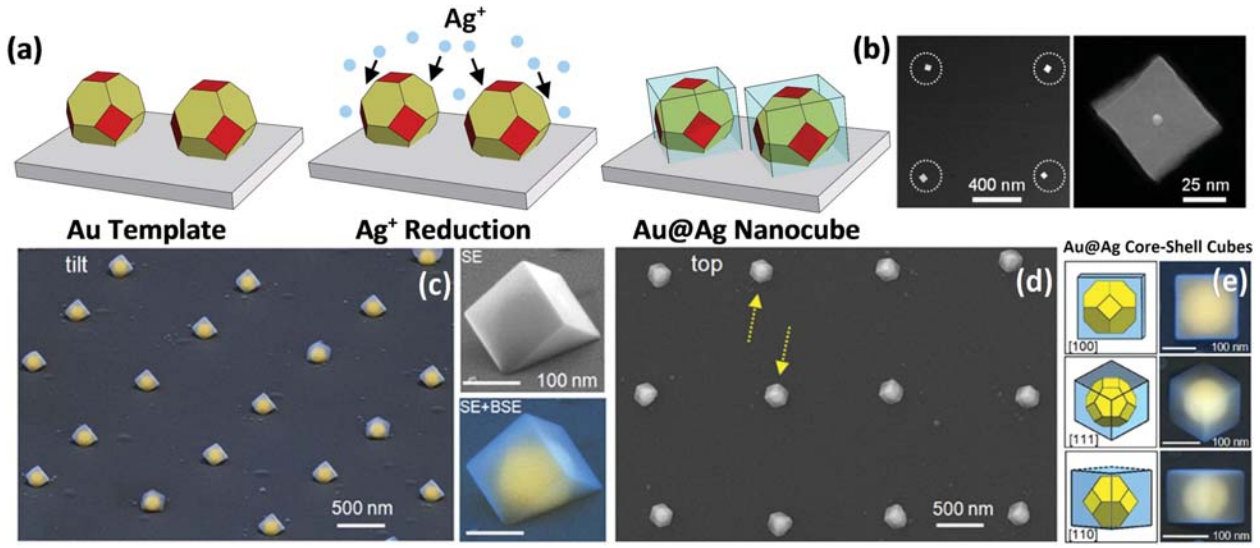

Figure 10. (a) Schematic of the process used to generate Au@Ag nanocubes through the reduction of Ag^{+} ions onto Wulff-shaped Au templates in the presence of a (100) capping agent. (b) HAADF–STEM images of [100]-oriented Au@Pd nanocubes. (c) Tilted- and (d) plan-view SEM images of [111]-oriented Au@Ag nanocubes where the inset shows a high magnification image of an individual structure. (e) Plan-view SEM images of Au@Ag nanocubes exhibiting three different orientations relative to the underlying substrate. (10b reproduced with permission from [130]. Copyright 2015 American Chemical Society.) (10c–e reproduced with permission from [131]. Copyright 2016 Wiley.)

The work demonstrated that reaction kinetics could be used to manipulate the shape of the final structure. The progression from fast, to moderate, to slow kinetics resulted in the transformation of the growth mode from conformal Ag deposition, to the formation of small Ag (111)-bounded pyramids on each of the (100) Au facets, to highly asymmetric structures characterized by a large hexagonal-shaped Ag protrusion off a single (100) Au facet. Liu *et al* [130] were the first to use facet-selective capping agents in a synthesis carried out at the liquid–substrate interface on arrayed templates. They used Au seeds, formed using the methods described in section 4.1 [123], to generate Au@Pd core–shell nanocubes using CTAB and ascorbic acid as the capping and reducing agent, respectively. Figure 10(b) shows the Au@Pd structures produced, where it should be recognized that the Au template is resting on the substrate surface as opposed to being located at the center of the cube. While their results are unquestionably impressive, the so-formed nanocubes did not show a consistent crystallographic orientation relative to underlying substrate, often displaying orientations other than the [100]-orientation shown in figure 10(b). Hajfathalian *et al* [131] overcame these alignment issues by incorporating epitaxy into the growth mode. Using [111]-oriented Au seeds heteroepitaxially aligned with a [0001]-oriented sapphire substrate, they generated Au@Ag core–shell nanocubes. Figures 10(c) and (d) show tilted- and top-view images of the Au@Ag structures formed, where the vast majority of the structures are [111]-oriented in one of two in-plane directions (denoted by yellow arrows). The high magnification image of an individual structure clearly shows asymmetries caused by the steric influences of the substrate, resulting in both a truncation of the cube at the substrate interface and a shell that is unable to envelop the Au template on all sides. While the vast majority of the structures were [111]-oriented, others exhibited [100] or [110] orientations (figure 10(e)).

4.2.2. Template-mediated synthesis through galvanic replacement, dealloying, and preferential etching. Some of the most complex colloidal metal nanostructures fabricated to date have subjected preformed templates to chemical environments that lead to their partial dissolution into the adjacent liquid medium. When carried out in a controlled manner, these subtractive processes can give rise to (i) hollow nanoshells, (ii) nanocages displaying a well-defined pattern of geometric openings, and (iii) highly porous structures with exceedingly high surface-to-volume ratios. Such reactions, which fall under the headings of galvanic replacement [137], dealloying [137, 138], and preferential etching [138, 139], have been widely practiced on solution-dispersed templates. While only a few demonstrations exist where these same reactions have been carried out using arrays of substrate-immobilized templates [41, 109, 117, 140–142], they have resulted in some of the most complex substrate-based nanostructures ever formed.

Galvanic replacement reactions are, by far, the most common synthetic method for realizing colloidal nanostructures with hollowed geometries. These template-mediated reduction–oxidation (redox) reactions are unique in that they involve both subtractive and additive processes. In the most widely used galvanic replacement reaction, a Ag template is exposed to an aqueous $HAuCl_4$ solution. The high electrochemical potential of the Au^{3+} ions gives rise to a spontaneous reaction that sees them reduced onto the solid Ag template as Ag^{+} ions are simultaneously released into the

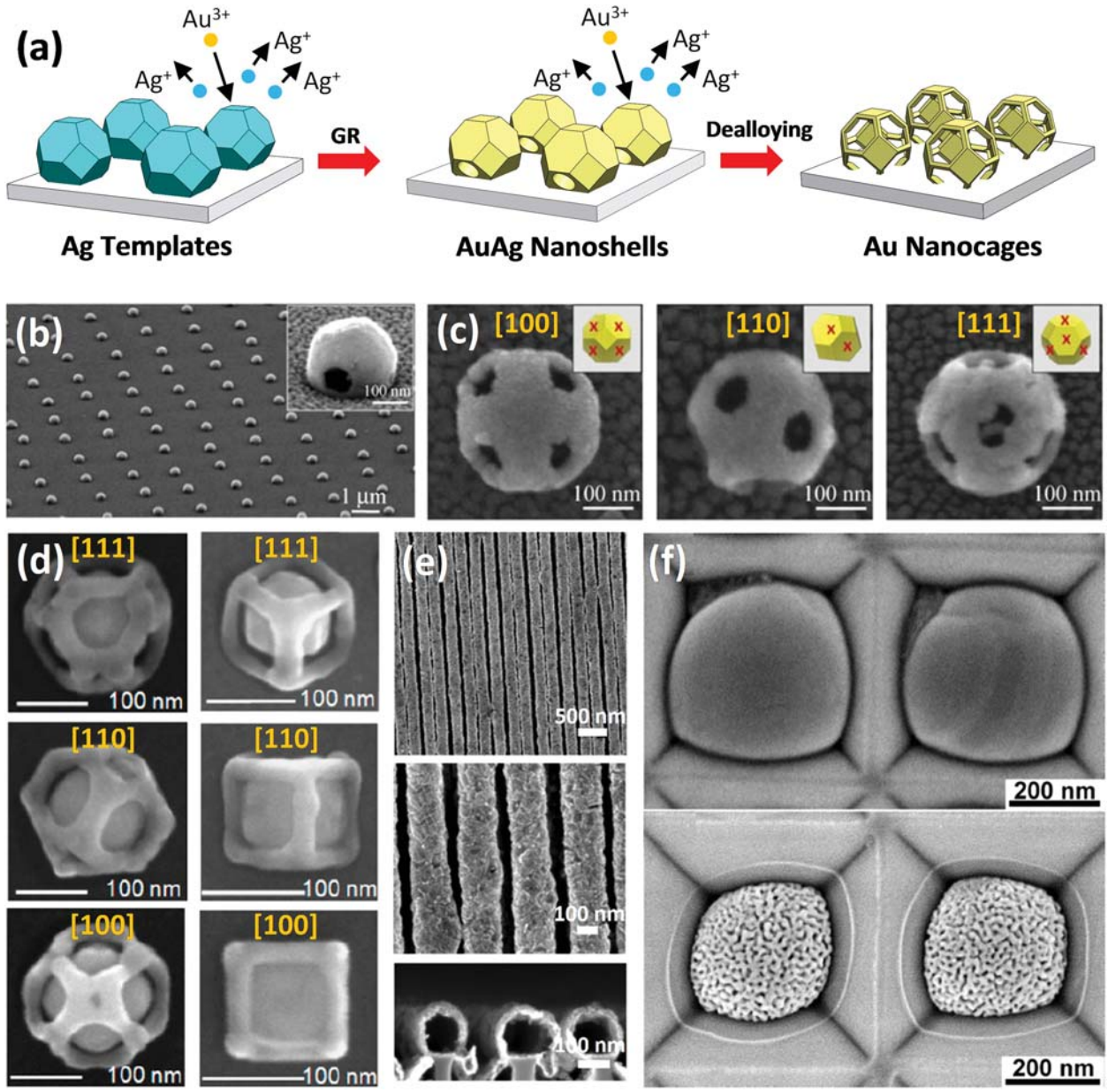

Figure 11. (a) Schematic showing Ag nanostructures that are first transformed into AuAg nanoshells through galvanic replacement (GR) with Au^{3+} and then further reconfigured into Au nanocages through dealloying. SEM images of AuAg (b) nanohuts, (c) nanocages, (d) nanocages confining a Wulff-shaped Pt core derived from templates with truncated octahedron (left) and cubic geometries (right), (e) nanotubes and (f) nanostructures before (top row) and after (bottom row) a Ag dealloying procedure. (11b, c reproduced with permission from [140]. Copyright 2014 Springer.) (11d reproduced with permission from [143]. Copyright 2016 American Chemical Society.) (11e reproduced with permission from [145]. Copyright 2016 American Chemical Society.) (11f reproduced with permission from [109]. Copyright 2012 Beilstein-Institut.)

solution according to the reaction:

$$3Ag(s) + Au^{3+}(aq) \rightarrow Au(s) + 3Ag^{+}(aq).$$

Over time the Ag template is transformed into a hollow nanoshell with a single opening through which the Ag^{+} ions exited (figure 11(a)). Alloying between the depositing Au and the underlying Ag template results in a AuAg nanoshell. Gilroy *et al* [140, 141] first demonstrated this reaction on arrays of Ag templates generated using the techniques described in section 3.3. The resulting structures, referred to as nanohuts (figure 11(b)), are unique in that the hollowed volume is enclosed by the substrate on the underside and by the AuAg nanoshell elsewhere. In a follow-up study [142], they demonstrated a substrate-based galvanic replacement reaction in which Pt^{4+} ions replaced templates of Ag, Cu, Ni, Co, and Pb, where near-pure Pt shells were obtained for the Ni and Co templates while all others showed some degree of alloying.

If the galvanic replacement of Ag templates with Au^{3+} is allowed to continue past the stage where the supply of pure

Ag is exhausted, then the reaction continues through the dealloying of the AuAg nanoshell, albeit at a much slower rate. The dealloying process, not only leads to a composition that trends toward pure Au, but also results in a morphological reconstruction (figure 11(a)) due to the volume loss resulting from the 3:1 Ag:Au replacement ratio. When dealloying was carried out on the substrate-based nanoshells shown in figure 11(b), it led to the formation of openings on each of the (111) faces [140]. As a result, Ag templates initially having [100], [110], and [111] orientations relative to the underlying substrate each gave rise to a unique nanocage geometry (figure 11(c)). Substrate-based structures of even greater complexity were synthesized by Hajfathalian *et al* [143] by performing galvanic replacement reactions on the X@Ag (X = Au, Pt, Pd) core–shell structures of varying geometries. In these reactions, the Ag shell is replaced while the core remains intact, resulting in an X@void@AuAg architecture. Figure 11(d) shows SEM images of the Pt@void@AuAg structures derived from core–shell templates with truncated octahedron and cubic geometries where each template orientation, once again, gives rise to a unique architecture. While the equivalent synthesis can be carried out using core–shell colloidal templates (i.e., the synthesis of nanorattles [144]), it is only the substrate-based synthesis that results in a well-defined gap between the core and the shell since both components are immobilized by the substrate. This unique feature makes these structures intriguing candidates for nanoreactor and sensing applications [143]. While not meeting the single crystal criteria for this review article, it is nevertheless noteworthy that El Mel *et al* [145] performed galvanic replacement reactions on lithographically-defined strips of polycrystalline Ag, becoming the first to demonstrate parallel rows of AuAg nanotubes over large areas (figure 11(e)).

Porous metals with nanostructured surfaces have been synthesized with bulk dimensions through the exposure of AuAg alloys to an etchant that selectively dissolves the Ag component [146]. In this case, dealloying occurs without the simultaneous plating that occurs in galvanic replacement reactions. Schaaf and co-workers have carried out the analogous synthesis on substrate-immobilized nanostructures [38, 95, 109]. In one demonstration, they exposed arrays of AuAg templates, formed using the substrate texturing technique described in section 3.2, to a nitric acid etch that selectively removes the Ag component [109]. The resulting structures (figure 11(f)) show a high degree of porosity where the specific surface area of the dealloyed structure is estimated to be as much as 10^5 times that of the starting template [38]. In another example of selective etching, Sundar *et al* [117] exposed AuGe heterostructures (section 3.3) to a selective Ge etch, a reaction yielding periodic arrays of Au nanoscrescents.

5. Concluding remarks

This review has documented recent progress in defining organized surfaces of complex nanostructures using methods that take advantage of the synergies formed when lithographic techniques are used in combination with assembly processes. These synthetic and fabrication routes have collectively given rise to an impressive collection of structures (table 1). The overall strategy has unequivocally proved successful in that it has given rise to periodic arrays of some of the most well-recognized nanostructure architectures as well as those that are unique to the substrate-based platform. The various approaches described herein, while linked by a general strategy and common goals, have nevertheless proceeded down distinctive synthetic and fabrication pathways that have seen them practiced in relative isolation from one another. When examined together, it is evident that each has its own advantages, but where no single technique represents a panacea to the challenges that lie ahead in the fields of nanofabrication and nanomanufacturing. With this being the case, we highlight some of the strengths of individual techniques as they relate to some of the most important parameters when forming organized surfaces of metal nanostructures.

An examination of the various directed assembly techniques reveal that its deficiencies are often rooted in the lithographic processes used or in the colloids that are assembled. The lithographic process is, in many instances, the determining factor in setting the minimum nanostructure size and spacing. It can also act as the bottleneck in terms of throughput. Assembly processes that, to some extent, mitigate these deficiencies are of particular note. In terms of nanostructure size, there are number of techniques that are able to produce nanostructures with dimensions that are well below the resolution limits of the lithographic process. Notable examples include: (i) the placement of colloids into lithographically-defined traps where a sizeable surface ligand [58] or auxiliary sidewall [52] acts to center a smaller nanostructure within a significantly larger trap, (ii) the use of sacrificial layers in dewetting processes that are able to greatly enhance the areal extent over which a single particle can agglomerate [121], and (iii) the deposition of attoliter droplets with sub-micrometer dimensions that act as chemical reactors from which much smaller nanostructures are derived [123]. While such processes are advantageous from the standpoint of fabricating small nanostructures there are, however, trade-offs in terms of the achievable array pitch and the existence of sizeable registration errors. Capillary assembly techniques have demonstrated the greatest potential for overcoming the limitations of conventional lithographic techniques in terms of placing nanostructures in close enough proximity to realize coupling phenomena [52, 54, 62]. These same techniques can, however, be hampered by the polydispersity of the colloid or a lack of phase and shape purity. The demonstration that capillary assembly techniques can be designed to offer some degree of filtering through shape-selectivity is, hence, notable [54]. In terms of throughput, directed assembly techniques utilizing NIL [147] or polymer pen lithography [125] have a distinct advantage. When capillary assembly is used in combination with microcontact printing, it becomes highly advantageous from the standpoint of placing arrayed structures on planar substrates of arbitrary composition and crystallinity [55].

Table 1. Summary of all the complex nanostructures described in this review.

Synthesis technique	Shape	Composition	Ligand	Reference
Capillary assembly	Nanorod	Au	CTAB	[52, 53, 62–65]
			CTAB/NaOL	[69]
	Nanocube	Ag, Au	CTAC, PVP	[54, 55]
	Nanoprism	Au	CTAB	[54]
	Multisegmented nanowire	Au–Ni–Au	CTAB	[56]
Chemically nanopatterned substrates	Nanorod	Au	CTAB	[42]
Templated dewetting	Hemisphere	AuPd		Current Study
	Intricate	Ni	None	[79, 101]
		Pd		[102]
	Spherical	CoPt, AuAg, AuNi		[76, 109, 110]
	Nanoprism	AuAg		[116]
	Hemispherical Janus	Au–Ge		[117]
	Wulff-shape	Pd		[118]
Syntheses in attoliter droplets	Hemisphere	PtNi, PtCo, PdNi, PdCo, CoNi, AuPd, AuAgPd	None	[123]
	Janus	Au–Ni		
Syntheses at the liquid–substrate interface	Wulff-shaped core–shell	Au@Ag, Au@Pt, Au@Pd	None	[129, 143]
	core–shell	Au@Ag, Au@Pt	CTAB	[130]
	Janus	Au–Ag	None	[129]
	Nanocube	Ag	Citrate	[131]
	Core–shell nanocube	Au@Pd	CTAB	[130]
		Au@Ag, Pt@Ag, Pd@Ag	Citrate	[131, 143]
	Hollow nanoshell	AuAg, Pt, PtAg, PtCu, PtNi, PtCo, PtPb	None	[140–142]
	Nanocage	AuAg		[141]
	Wulff-shaped core-void-shell (or cube, frame)	X@void@AuAg, X = Au, Pt, Pd	None	[143]
	Cube-shaped core-void-shell (or cube, frame)		Citrate	[143]
	Nanotube	AuAg	None	[145]
	Nanoporous sphere	Au		[109]
	Nanocrescent	Au, Ag		[117]

With respect to the arrayed nanostructures, it is highly desirable to exert control over their architecture, size, orientation, crystallinity, and surface quality. Template-mediated syntheses carried out at the liquid–substrate interface [41] are unmatched in terms of exerting architectural control. It is the only methodology that has led to the formation of hollowed structures and also allows for heterogeneous depositions controlled by facet-selective capping agents. With a rich and powerful colloidal chemistry at its disposal, this approach is likely to remain unrivalled in this regard. While many directed assembly techniques lend themselves to nanostructures of various sizes, it is only the tip-directed assembly methods [123] that have demonstrated mastery over the precise placement of sub-20 nm alloyed nanostructures into organized patterns. Control over nanostructure orientation is most readily achieved using capillary assembly [53] or through techniques promoting an epitaxial relationship between the nanostructure and a crystalline substrate [41]. The elevated temperatures used in templated dewetting techniques [35–39] result in the highest degree of crystallinity, and because no surface ligands are required, often express pristine surfaces. It is, however, noted that even those techniques that utilize colloids have the opportunity to remove nanostructure surface ligands through cleaning procedures put in place once the structures are immobilized on the substrate surface. With such ligands proving detrimental to numerous properties [24–29], such procedures can result in substrate-bound structures that express greater functionality than the colloidal structures from which they were derived.

The merger of lithographic and self-assembly processes has resulted in a broad range of directed assembly techniques with capabilities that transcend those of constituent

approaches. With numerous proof-of-principle demonstrations of the directed assembly of complex metal nanostructures now in place, the field is poised to face the challenges and opportunities associated with achieving greater control over synthesis and fabrication, device prototyping, and a higher degree of integration with wafer-based processing and characterization techniques. We very much hope that this review, by bringing together a diverse collection of synthetic and lithographic practices, will spur interest, spawn new ideas, and add to the excitement of this active and vibrant field.

Acknowledgments

This work is supported by National Science Foundation Awards (CMMI- 1707595 and DMR-1707593) to SN. The authors also wish to acknowledge the efforts of Pouyan Farzinpour, Aarthi Sundar, Kyle Gilroy, and Maryam Hajfathalian, all former PhD students who greatly contributed to this research direction and on which portions of this review are based. Spencer Golze is acknowledged for the nanoimprints used to generate the results in figure 6(b). We thank Ian Lightcap and the ND Energy Materials Characterization Facility for the use of the Bruker D8 Advance Davinci Diffractometer.

References

[1] Xi C, Marina P F, Xia H and Wang D 2015 Directed self-assembly of gold nanoparticles into plasmonic chains *Soft Matter* **11** 4562–71
[2] Zhang S-Y, Regulacio M D and Han M-Y 2014 Self-assembly of colloidal one-dimensional nanocrystals *Chem. Soc. Rev.* **43** 2301–23
[3] Zhang J, Li Y, Zhang X and Bai Y 2010 Colloidal self-assembly meets nanofabrication: from two-dimensional colloidal crystals to nanostructure arrays *Adv. Mater.* **22** 4249–69
[4] Jones M R, Osberg K D, Macfarlane R J, Langille M R and Mirkin C A 2011 Templated techniques for the synthesis and assembly of plasmonic nanostructures *Chem. Rev.* **111** 3736–827
[5] Kinge S, Crego-Calama M and Reinhoudt D N 2008 Self-assembling nanoparticles at surfaces and interfaces *Chem. Phys. Chem.* **9** 20–42
[6] Ariga K, Yamauchi Y, Mori T and Hill J P 2013 25th anniversary article: what can be done with the Langmuir–Blodgett method? Recent developments and its critical role in materials science *Adv. Mater.* **25** 6477–512
[7] Ross M B, Ku J C, Lee B, Mirkin C A and Schatz G C 2016 Plasmonic metallurgy enabled by DNA *Adv. Mater.* **28** 2790–4
[8] Young K L, Ross M B, Blaber M G, Rycenga M, Jones M R, Zhang C, Senesi A J, Lee B, Schatz G C and Mirkin C A 2014 Using DNA to design plasmonic metamaterials with tunable optical properties *Adv. Mater.* **26** 653–9
[9] Tan S J, Campolongo M J, Luo D and Cheng W 2011 Building plasmonic nanostructures with DNA 2011 *Nat. Nanotechnol.* **6** 268–76
[10] Vogel N, Retsch M, Fustin C-A, del Campo A and Jonas U 2015 Advances in colloidal assembly: the design of structure and hierarchy in two and three dimensions *Chem. Rev.* **115** 6265−6311
[11] Barrow S J, Funston A M, Wei X and Mulvaney P 2013 DNA-directed self-assembly and optical properties of discrete 1D, 2D and 3D plasmonic structures *Nano Today* **8** 138–67
[12] Boles M A, Engel M and Talpin D V 2016 Self-assembly of colloidal nanocrystals: from intricate structures to functional materials *Chem. Rev.* **116** 11220–89
[13] Henzie J, Andrews S C, Ling X Y, Li Z and Yang P 2013 Oriented assembly of polyhedral plasmonic nanoparticle clusters *Proc. Natl Acad. Sci. USA* **110** 6640–5
[14] Liddle J A and Gallatin G M 2016 Nanomanufacturing: a perspective *ACS Nano* **10** 2995−3014
[15] Millstone J E, Hurst S J, Métraux G S, Cutler J I and Mirkin C A 2009 Colloidal gold and silver triangular nanoprisms *Small* **5** 646–64
[16] Siegfried T, Ekinci Y, Martin O J F and Sigg H 2013 Engineering metal adhesion layers that do not deteriorate plasmon resonances *ACS Nano* **7** 2751–7
[17] Soukoulis C M and Wegener M 2011 Past achievements and future challenges in the development of three-dimensional photonic metamaterials *Nat. Photon.* **5** 523–30
[18] Xia Y, Gilroy K D, Peng H-C and Xia X 2017 Seed-mediated growth of colloidal nanocrystals *Angew. Chem., Int. Ed.* **56** 60–95
[19] Gilroy K D, Ruditskiy A, Peng H-C, Qin D and Xia Y 2016 Bimetallic nanocrystals: syntheses, properties, and applications *Chem. Rev.* **116** 10414–72
[20] Personick M L and Mirkin C A 2013 Making sense of the mayhem behind shape control in the synthesis of gold nanoparticles *J. Am. Chem. Soc.* **135** 18238–47
[21] Xia Y, Xiong Y, Lim B and Skrabalak S E 2009 Shape-controlled synthesis of metal nanocrystals: simple chemistry meets complex physics? *Angew. Chem., Int. Ed.* **48** 60–103
[22] Bishop K J M, Wilmer C E, Soh S and Grzybowski B A 2009 Nanoscale forces and their uses in self-assembly *Small* **14** 1600–30
[23] Pincella F, Isozaki K and Miki K 2014 A visible light-driven plasmonic photocatalyst *Light: Sci. Appl.* **3** e133
[24] Li Z, Mao W, Devadas M S and Hartland G V 2015 Absorption spectroscopy of single optically trapped gold nanorods *Nano Lett.* **15** 7731–5
[25] Prati L and Villa A 2014 Gold colloids: from quasi-homogeneous to heterogeneous catalytic systems *Acc. Chem. Res.* **47** 855–63
[26] Jenkins S V, Chen S and Chen J 2015 Gold–copper alloyed nanorods for metal-catalyzed organic reactions: implication of surface ligands on nanoparticle-based heterogeneous catalysis *Tetrahedron Lett.* **56** 3368–72
[27] Liu X, Li C, Xu J, Lv J, Zhu M, Guo Y, Cui S, Liu H, Wang S and Li Y 2008 Surfactant-free synthesis and functionalization of highly fluorescent gold quantum dots *J. Phys. Chem.* C **112** 10778–83
[28] Dar M I, Sampath S and Shivashankar S A 2012 Microwave-assisted, surfactant-free synthesis of air-stable copper nanostructures and their SERS study *J. Mater. Chem.* **22** 22418–23
[29] Aruda K O, Tagliazucchi M, Sweeney C M, Hannah D C, Schatz G C and Weiss E A 2013 Identification of parameters through which surface chemistry determines the life-times of hot electrons in small Au nanoparticles *Proc. Natl Acad. Sci. USA* **110** 4212–7
[30] Koh S J 2007 Strategies for controlled placement of nanoscale building blocks *Nanoscale Res. Lett.* **2** 519–45
[31] Tian D, Song Y and Jiangab L 2013 Patterning of controllable surface wettability for printing techniques *Chem. Soc. Rev.* **42** 5184–209

[32] Fernandez Y A D, Gschneidner T A, Wadell C, Fornander L H, Avila S L, Langhammer C, Westerlund F and Moth-Poulsen K 2014 The conquest of middle-earth: combining top-down and bottom-up nanofabrication for constructing nanoparticle devices *Nanoscale* **6** 14605–16

[33] Hamon C and Liz-Marzán L M 2015 Hierarchical assembly of plasmonic nanoparticles *Chem. Eur. J.* **21** 9956–63

[34] Rycenga M, Camargo P H C and Xia Y 2009 Template-assisted self-assembly: a versatile approach to complex micro- and nanostructures *Soft Matter* **5** 1129–36

[35] Altomare M, Nguyen N T and Schmuki P 2016 Templated dewetting: designing entirely self-organized platforms for photocatalysis *Chem. Sci.* **7** 6865–86

[36] Leroy F, Borowik Ł, Cheynis F, Almadori Y, Curiotto S, Trautmann M, Barbé J C and Müller P 2016 How to control solid state dewetting: a short review *Surf. Sci. Rep.* **71** 391–409

[37] Ruffino F and Grimaldi M G 2015 Controlled dewetting as fabrication and patterning strategy for metal nanostructures *Phys. Status Solidi* a **212** 1662–84

[38] Wang D and Schaaf P 2013 Solid-state dewetting for fabrication of metallic nanoparticles and influences of nanostructured substrates and dealloying *Phys. Status Solidi* a **210** 1544–51

[39] Thompson C V 2012 Solid-state dewetting of thin films *Annu. Rev. Mater. Res.* **42** 399–434

[40] Guardingo M, Busqué F and Ruiz-Molina D 2016 Reactions in ultra-small droplets by tip-assisted chemistry *Chem. Commun.* **52** 11617–26

[41] Neretina S, Hughes R A, Gilroy K D and Hajfathalian M 2016 Noble metal nanostructure synthesis at the liquid −substrate interface: new structures, new insights, and new possibilities *Acc. Chem. Res.* **49** 2243−250

[42] Nepal D, Onses M S, Park K, Jespersen M, Thode C J, Nealey P F and Vaia R A 2012 Control over position, orientation, and spacing of arrays of gold nanorods using chemically nanopatterned surfaces and tailored particle-particle-surface interactions *ACS Nano* **6** 5693–701

[43] Ahmed W, Glass C, Kooij E S and van Ruitenbeek J M 2014 Tuning the oriented deposition of gold nanorods on patterned substrates *Nanotechnology* **25** 035301

[44] Cui Y, Björk M T, Liddle J A, Sönnichsen C, Boussert B and Alivastos A P 2004 Integration of colloidal nanocrystals into lithographically patterned devices *Nano Lett.* **4** 1093–8

[45] Ni S, Leemann J, Wolf H and Isa L 2015 Insights into mechanisms of capillary assembly *Faraday Discuss.* **181** 225–42

[46] Hung A M, Micheel C M, Bozano L D, Osterbur L W, Wallraff G M and Cha J N 2009 Large-area spatially ordered arrays of gold nanoparticles directed by lithographically confined DNA origami *Nat. Nanotechnol.* **5** 121–6

[47] Jiang L, Sun Y, Nowak C, Kibrom A, Zou C, Ma J, Fuchs H, Li S, Chi L and Chen X 2011 Patterning of plasmonic nanoparticles into multiplexed one-dimensional arrays based on spatially modulated electrostatic potential *ACS Nano* **5** 8288–94

[48] Lee C S, Lee H and Westervelt R M 2001 Microelectromagnets for the control of magnetic nanoparticles *Appl. Phys. Lett.* **79** 3308–10

[49] Deegan R D, Bakajin O, Dupont T F, Huber G, Nagel S R and Witten T A 1997 Capillary flow as the cause of ring stains from dried liquid drops *Nature* **389** 827–9

[50] Han W and Lin Z 2012 Learning from 'coffee rings': ordered structures enabled by controlled evaporative self-assembly *Angew. Chem., Int. Ed* **51** 1534–46

[51] Malaquin L, Kraus T, Schmid H, Delamarche E and Wolf H 2007 Controlled particle placement through convective and capillary assembly *Langmuir* **23** 11513–21

[52] Flauraud V, Mastrangeli M, Bernasconi G D, Butet J, Alexander D T L, Shahrabi E, Martin O J F and Brugger J 2017 Nanoscale topographical control of capillary assembly of nanoparticles *Nat. Nanotechnol.* **12** 73–80

[53] Kuemin C, Nowack L, Bozano L, Spencer N D and Wolf H 2012 Oriented assembly of gold nanorods on the single-particle level *Adv. Funct. Mater.* **22** 702–8

[54] Zhou Y, Zhou X, Park D J, Torabi K, Brown K A, Jones M R, Zhang C, Schatz G C and Mirkin C A 2014 Shape-selective deposition and assembly of anisotropic nanoparticles *Nano Lett.* **14** 2157–61

[55] Kraus T, Malaquin L, Schmid H, Riess W, Spencer N D and Wolf H 2007 Nanoparticle printing with single-particle resolution *Nat. Nanotechnol.* **2** 570–6

[56] Zhou X, Zhou Y, Ku J C, Zhang C and Mirkin C A 2014 Capillary force-driven, large-area alignment of multi-segmented nanowires *ACS Nano* **8** 1511–6

[57] Gordon M J and Peyrade D 2006 Separation of colloidal nanoparticles using capillary immersion forces *Appl. Phys. Lett.* **89** 053112

[58] Jiang L, Chen X, Lu N and Chi L 2014 Spatially confined assembly of nanoparticles *Acc. Chem. Res.* **47** 3009–17

[59] Fan J A, Bao K, Sun L, Bao J, Manoharan V N, Nordlander P and Capasso F 2012 Plasmonic mode engineering with templated self-assembled nanoclusters *Nano Lett.* **12** 5318–24

[60] Rivera T P, Lecarme O, Hartmann J, Inglebert R L and Peyrade D 2009 Spectroscopic studies of plasmonic interaction in colloidal dimers fabricated by convective-capillary force assembly *Microelectron. Eng.* **86** 1089–92

[61] Greybush N J, Liberal I, Malassis L, Kikkawa J M, Engheta N, Murray C B and Kagan C R 2017 Plasmon resonances in self-assembled two-dimensional Au manocrystal metamolecules *ACS Nano* **11** 2917–27

[62] Rey A, Billardon G, Lörtscher E, Moth-Poulsen K, Stuhr-Hansen N, Wolf H, Bjørnholm T, Stemmer A and Riel H 2013 Deterministic assembly of linear gold nanorod chains as a platform for nanoscale applications *Nanoscale* **5** 8680–8

[63] Kuemin C, Stutz R, Spencer N D and Wolf H 2011 Precise placement of gold nanorods by capillary assembly *Langmuir* **27** 6305–10

[64] Holzner F, Kuemin C, Paul P, Hedrick J L, Wolf H, Spencer N D, Duerig U and Knoll A W 2011 Directed placement of gold nanorods using a removable template for guided assembly *Nano Lett.* **11** 3957–62

[65] Tebbe M *et al* 2015 Optically anisotropic substrates via wrinkle-assisted convective assembly of gold nanorods on macroscopic areas *Faraday Discuss.* **181** 243–60

[66] Tong Q, Malachosky E W, Raybin J, Guyot-Sionnest P and Sibener S J 2014 End-to-end alignment of gold nanorods on topographically enhanced, cylinder forming diblock copolymer templates and their surface enhanced Raman scattering properties *J. Phys. Chem.* C **118** 19259–65

[67] Nikoobakht B and El-Sayed M A 2001 Evidence for bilayer assembly of cationic surfactants on the surface of gold nanorods *Langmuir* **17** 6368–74

[68] Walker D A, Browne K P, Kowalcsyk B and Grzybowski B A 2010 Self-assembly of nanotriangle superlattices facilitated by repulsive electrostatic interactions *Angew. Chem., Int. Ed.* **49** 6760–3

[69] Greybush N J, Saboktakin M, Ye X, Giovampaola C D, Oh S J, Berry N E, Engheta N, Murray C B and Kagan C R 2014 Plasmon-enhanced upconversion luminescence in single nanophosphor-nanorod heterodimers formed through template-assisted self-assembly *ACS Nano* **8** 9482–91

[70] Ma L-C, Subramanian R, Huang H-W, Ray V, Kim C-U and Koh S J 2007 Electrostatic funneling for precise nanoparticle

placement: a route to wafer-scale integration *Nano Lett.* **7** 439–45
[71] Liu Z, Chang T, Huang H and Lu Bai 2016 Cross-linked block copolymer templated assembly of nanoparticle arrays with high density and position selectivity *Appl. Surf. Sci.* **384** 400–5
[72] Liu X, Biswas S, Jarrett J W, Poutrina E, Urbas A, Knappenberger K L Jr, Vaia R A and Nealey P F 2015 Deterministic construction of plasmonic heterostructures in well-organized arrays for nanophotonic materials *Adv. Mater.* **27** 7314–9
[73] Jiang L, Wang W, Fuchs H and Chi L 2009 One-dimensional arrangement of gold nanoparticles with tunable interparticle distance *Small* **5** 2819–22
[74] Owusu-Ansah E, Horwood C A, El-Sayed H A, Birss V I and Shi Y J 2015 A method for the formation of Pt metal nanoparticle arrays using nanosecond pulsed laser dewetting *Appl. Phys. Lett.* **106** 203103
[75] Roberts N A, Fowlkes J D, Mahady K, Afkhami S, Kondic L and Rack P D 2013 Directed assembly of one- and two-dimensional nanoparticle arrays from pulsed laser induced dewetting of square waveforms *ACS Appl. Mater. Interfaces* **5** 4450–6
[76] Oh Y-J, Kim J-H, Thompson C V and Ross C A 2013 Templated assembly of Co–Pt nanoparticles via thermal and laser-induced dewetting of bilayer metal films *Nanoscale* **5** 401–7
[77] Fowlkes J D, Kondic L, Diez J, Wu Y and Rack P D 2011 Self-assembly versus directed assembly of nanoparticles via pulsed laser induced dewetting of patterned films *Nano Lett.* **11** 2478–85
[78] Wu Y, Fowlkes J D, Rack P D, Diez J A and Kondic L 2010 On the breakup of patterned nanoscale copper rings into droplets via pulsed-laser-induced dewetting: competing liquid-phase instability and transport mechanisms *Langmuir* **26** 11972–9
[79] Rack P D, Guan Y, Fowlkes J D, Melechko A V and Simpson M L 2008 Pulsed laser dewetting of patterned thin metal films: a means of directed assembly *Appl. Phys. Lett.* **92** 223108
[80] Lian J, Wang L, Sun X, Yu Q and Ewing R C 2006 Patterning metallic nanostructures by ion-beam-induced dewetting and rayleigh instability *Nano Lett.* **6** 1047–52
[81] Kojima Y and Kato T 2008 Nanoparticle formation in Au thin films by electron-beam-induced dewetting *Nanotechnology* **19** 255605
[82] Farzinpour P, Sundar A, Gilroy K D, Eskin Z E, Hughes R A and Neretina S 2012 Altering the dewetting characteristics of ultrathin gold and silver films using a sacrificial antimony layer *Nanotechnology* **23** 495604
[83] Müller C M and Spolenak R 2010 Microstructure evolution during dewetting in thin Au films *Acta Mater.* **58** 6035–45
[84] Leroy F, Cheynis F, Passanante T and Muller P 2012 Dynamics, anisotropy, and stability of silicon-on-insulator dewetting fronts *Phys. Rev.* B **85** 195414
[85] Devenyi G A, Li J F, Hughes R A, Shi A C, Mascher P and Preston J S 2009 Epitaxially driven formation of intricate supported gold nanostructures on a lattice-matched oxide substrate *Nano Lett.* **9** 4258–63
[86] Silly F, Powell A C, Martin M G and Castell M R 2005 Growth shapes of supported Pd nanocrystals on $SrTiO_3$ (001) *Phys. Rev.* B **72** 165403
[87] Majdi T, Zhu G-Z, Carvalho J, Jarvis V, Meinander K, Britten J F, Botton G and Preston J S 2015 Evidence for an equilibrium epitaxial complexion at the Au–$MgAl_2O_4$ interface *Appl. Phys. Lett.* **107** 241601
[88] Hajjar S *et al* 2011 Morphology and composition of Au catalysts on Ge(111) obtained by thermal dewetting *Phys. Rev.* B **84** 125325
[89] Giermann A L and Thompson C V 2005 Solid-state dewetting for ordered arrays of crystallographically oriented metal particles *Appl. Phys. Lett.* **86** 121903
[90] Kan W and Wong H 2005 Fingering instability of a retracting solid film edge *J. Appl. Phys.* **97** 043515
[91] Henry C R 2005 Morphology of supported nanoparticles *Prog. Surf. Sci.* **80** 92–116
[92] Kim D, Giermann A L and Thompson C V 2009 Solid-state dewetting of patterned thin films *Appl. Phys. Lett.* **95** 251903
[93] Müller C M, Mornaghini F C F and Spolenak R 2008 Ordered arrays of faceted gold nanoparticles obtained by dewetting and nanosphere lithography *Nanotechnology* **19** 485306
[94] Garozzo C, Puglisi R A, Bongiorno C, Scalese S, Rimini E and Lombardo S 2011 Selective diffusion of gold nanodots on nanopatterned substrates realized by self-assembly of diblock copolymers *J. Mater. Res.* **26** 240–6
[95] Wang D and Schaaf P 2012 Nanoporous gold nanoparticles *J. Mater. Chem.* **22** 5344–8
[96] Seo O, Oh S A, Lee J Y, Ha S S, Kim J M, Choi J W, Kim J-W, Kang H C and Noh D Y 2016 Controlling the alloy composition of PtNi nanocrystals using solid-state dewetting of bilayer films *J. Alloy Compd.* **667** 141–5
[97] Müller C M and Spolenak R 2013 Dewetting of Au and AuPt alloy films: a dewetting zone model *J. Appl. Phys.* **113** 094301
[98] Herz A, Friak M, Rossberg D, Hentschel M, Theska F, Wang D, Holec W D, Sob M, Schneeweiss O and Schaaf P 2015 Facet-controlled phase separation in supersaturated Au–Ni nanoparticles upon shape equilibration *Appl. Phys. Lett.* **107** 073109
[99] Amram D and Rabkin E 2014 Core(Fe)–shell(Au) nanoparticles obtained from thin Fe/Au bilayers employing surface segregation *ACS Nano* **8** 10687–93
[100] Esterina R, Liu X M, Adeyeye A O, Ross C A and Choi W K 2015 Solid-state dewetting of magnetic binary multilayer thin films *J. Appl. Phys.* **118** 144902
[101] Ye J and Thompson C V 2011 Templated solid-state dewetting to controllably produce complex patterns *Adv. Mater.* **23** 1567–71
[102] Ye J 2015 Fabrication of ordered arrays of micro- and nanoscale features with control over their shape and size via templated solid-state dewetting *Sci. Rep.* **5** 09823
[103] Giermann A L and Thompson C V 2011 Requirements for graphoepitaxial alignment through solid-state dewetting of Au films *J. Appl. Phys.* **109** 083520
[104] Wang D, Ji R and Schaaf P 2011 Formation of precise 2D Au particle arrays via thermally induced dewetting on pre-patterned substrates *Beilstein J. Nanotechnol.* **2** 318–26
[105] Choi W K, Liew T H, Chew H G, Zheng F, Thompson C V, Wang Y, Hong M H, Wang X D, Li L and Yun J 2008 A combined top-down and bottom-up approach for precise placement of metal nanoparticles on silicon *Small* **4** 330–3
[106] Le Bris A, Maloum F, Teisseire J and Sorin F 2014 Self-organized ordered silver nanoparticle arrays obtained by solid state dewetting *Appl. Phys. Lett.* **105** 203102
[107] Oh Y-J, Ross C A, Jung Y S, Wang Y and Thompson C V 2009 Cobalt nanoparticle arrays made by templated solid-state dewetting *Small* **5** 860–5
[108] Choe H J, Kwon S-H, Choe C, Lee J-J and Woo C-H 2016 Sn microparticles made by plasma-induced dewetting *Thin Solid Films* **620** 165–9
[109] Wang D, Ji R, Albrecht A and Schaaf P 2012 Ordered arrays of nanoporous gold nanoparticles *Beilstein J. Nanotechnol.* **3** 651–7
[110] Herz A, Wang D and Schaaf P 2014 Dewetting of Au/Ni bilayer films on prepatterned substrates and the formation of arrays of supersaturated Au–Ni nanoparticles *J. Vac. Sci. Technol.* B **32** 021802

[111] Hong S, Kang T, Choi D, Choi Y and Lee L P 2012 Self-assembled three-dimensional nanocrown array *ACS Nano* **6** 5803–8

[112] Meshot E R, Zhao Z, Lua W and Hart A J 2014 Self-ordering of small-diameter metal nanoparticles by dewetting on hexagonal mesh templates *Nanoscale* **6** 10106–12

[113] Yang S, Xu F, Ostendorp S, Wilde G, Zhao H and Lei Y 2011 Template-confined dewetting process to surface nanopatterns: fabrication, structural tunability, and structure-related properties *Adv. Funct. Mater.* **21** 2446–55

[114] Wang L-W, Cheng C-F, Liao J-W, Wang C-Y, Wang D-S, Huang K-F, Lin T-Y, Ho R-M, Chen L-J and Lai C-H 2016 Thermal dewetting with a chemically heterogeneous nano-template for self-assembled $L1_0$ FePt nanoparticle arrays *Nanoscale* **8** 3926–35

[115] Krupinski M, Perzanowski M, Zarzycki A, Zabila Y and Marszałek M 2015 Ordered FePdCu nanoisland arrays made by templated solid-state dewetting *Nanotechnology* **26** 425301

[116] Gilroy K D, Sundar A, Hajfathalian M, Yaghoubzade A, Tan T, Sil D, Borguet E, Hughes R A and Neretina S 2015 Transformation of truncated gold octahedrons into triangular nanoprisms through the heterogeneous nucleation of silver *Nanoscale* **7** 6827–35

[117] Sundar A, Farzinpour P, Gilroy K D, Tan T, Hughes R A and Neretina S 2014 Eutectic combinations as a pathway to the formation of substrate-based Au–Ge heterodimers and hollowed Au nanocrescents with tunable optical properties *Small* **10** 3379–88

[118] Sundar A, Farzinpour P, Gilroy K D, Tan T, Hughes R A and Neretina S 2013 Organized surfaces of highly faceted single-crystal palladium structures seeded by sacrificial templates *Cryst. Growth Des.* **13** 3847–51

[119] Hajfathalian M, Gilroy K D, Yaghoubzade A, Sundar A, Tan T, Hughes R A and Neretina S 2015 Photocatalytic enhancements to the reduction of 4-nitrophenol by resonantly excited triangular gold–copper nanostructures *J. Phys. Chem.* C **119** 17308–15

[120] Sundar A, Hughes R A, Farzinpour P, Gilroy K D, Devenyi G A, Preston J S and Neretina S 2012 Manipulating the size distribution of supported gold nanostructures *Appl. Phys. Lett.* **100** 013111

[121] Farzinpour P, Sundar A, Gilroy K D, Eskin Z E, Hughes R A and Neretina S 2015 Dynamic templating: a large area processing route for the assembly of periodic arrays of sub-micrometer and nanoscale structures *Nanoscale* **5** 1929–38

[122] Baletto F, Mottet C and Ferrando R 2000 Molecular dynamics simulations of surface diffusion and growth on silver and gold clusters *Surf. Sci.* **446** 31–45

[123] Chen P-C *et al* 2015 Tip-directed synthesis of multimetallic nanoparticles *J. Am. Chem. Soc.* **137** 9167–73

[124] Brown K A, Eichelsdoerfer D J, Liao X, He S and Mirkin C A 2014 Material transport in dip-pen nanolithography *Front. Phys.* **9** 385–97

[125] Huo F, Zheng Z, Zheng G, Giam L R, Zhang H and Mirkin C A 2008 Polymer pen lithography *Science* **321** 1658–60

[126] Chai J, Huo F, Zheng Z, Giam L R, Shim W and Mirkin C A 2010 Scanning probe block copolymer lithography *Proc. Natl Acad. Sci. USA* **107** 20202–6

[127] Liua G, Eichelsdoerfer D J, Rasin B, Zhou Y, Brown K A, Liao X and Mirkin C A 2013 Delineating the pathways for the site-directed synthesis of individual nanoparticles on surfaces *Proc. Natl Acad. Sci. USA* **110** 887–91

[128] Wu J *et al* 2014 *In situ* synthesis of large-area single sub-10 nm nanoparticle arrays by polymer pen lithography *Nanoscale* **6** 749–52

[129] Gilroy K D, Hughes R A and Neretina S 2014 Kinetically controlled nucleation of silver on surfactant-free gold seeds *J. Am. Chem. Soc.* **136** 15337–45

[130] Liu G, Zhang C, Wu J and Mirkin C A 2015 Using scanning-probe block copolymer lithography and electron microscopy to track shape evolution in multimetallic nanoclusters *ACS Nano* **9** 12137–45

[131] Hajfathalian M, Gilroy K D, Hughes R A and Neretina S 2016 Citrate-induced nanocubes: a reexamination of the role of citrate as a shape-directing capping agent for Ag-based nanostructures *Small* **12** 3444–52

[132] Weiner R G, Kunz M R and Skrabalak S E 2015 Seeding a new kind of garden: synthesis of architecturally defined multimetallic nanostructures by seed-mediated co-reduction *Acc. Chem. Res.* **48** 2688–95

[133] Xia Y, Xia X and Peng H–C 2015 Shape-controlled synthesis of colloidal metal nanocrystals: thermodynamic *versus* kinetic products *J. Am. Chem. Soc.* **137** 7947–66

[134] Zhu C, Zeng J, Tao J, Johnson M C, Schmidt–Krey I, Blubaugh L, Zhu Y, Gu Z and Xia Y 2012 Kinetically controlled overgrowth of Ag or Au on Pd nanocrystal seeds: from hybrid dimers to nonconcentric and concentric bimetallic nanocrystals *J. Am. Chem. Soc.* **134** 15822–31

[135] Xia X, Zeng J, Zhang Q, Moran C H and Xia Y 2012 Recent developments in shape-controlled synthesis of silver nanocrystals *J. Phys. Chem. C* **116** 21647–56

[136] Gilroy K D, Peng H-C, Yang X, Ruditskiy A and Xia Y 2017 Symmetry breaking during nanocrystal growth *Chem. Commun.* **53** 4530–41

[137] Xia X, Wang Y, Ruditskiy A and Xia Y 2013 25th anniversary article: galvanic replacement: a simple and versatile route to hollow nanostructures with tunable and well-controlled properties *Adv. Mater.* **25** 6313–33

[138] Fang Z, Wang Y, Liu C, Chen S, Sang W, Wang C and Zeng J 2015 Rational design of metal nanoframes for catalysis and plasmonics *Small* **11** 2593–605

[139] Li J, Sun X and Qin D 2016 Ag-enriched Ag–Pd bimetallic nanoframes and their catalytic properties *ChemNanoMat* **2** 494–9

[140] Gilroy K D, Sundar A, Farzinpour P, Hughes R A and Neretina S 2014 Mechanistic study of substrate-based galvanic replacement reactions *Nano Res.* **7** 365–79

[141] Gilroy K D, Farzinpour P, Sundar A, Tan T, Hughes R A and Neretina S 2013 Substrate-based galvanic replacement reactions carried out on heteroepitaxially formed silver templates *Nano Res.* **6** 418–28

[142] Gilroy K D, Farzinpour P, Sundar A, Hughes R A and Neretina S 2014 Sacrificial templates for galvanic replacement reactions: design criteria for the synthesis of pure Pt nanoshells with a smooth surface morphology *Chem. Mater.* **26** 3340–7

[143] Hajfathalian M, Gilroy K D, Golze S D, Yaghoubzade A, Menumerov E, Hughes R A and Neretina S A 2016 Wulff in a cage: the confinement of substrate-based structures in plasmonic nanoshells, nanocages, and nanoframes using galvanic replacement *ACS Nano* **10** 6354–62

[144] Sun Y, Wiley B, Li Z-Y and Xia Y 2004 Synthesis and optical properties of nanorattles and multiple-walled nanoshells/nanotubes made of metal alloys *J. Am. Chem. Soc.* **126** 9399–406

[145] El Mel A-A *et al* 2016 Galvanic replacement reaction: a route to highly ordered bimetallic nanotubes *J. Phys. Chem.* C **120** 17652–9

[146] Erlebacher J, Aziz M J, Karma A, Dimitrov N and Sieradzki K 2001 Evolution of nanoporosity in dealloying *Nature* **410** 450–3

[147] Guo L J 2007 Nanoimprint lithography: methods and material requirements *Adv. Mater.* **19** 495–513